Redox Biology 97 (2026) 104404

Contents lists available at ScienceDirect

Redox Biology

journal homepage: www.elsevier.com/locate/redox

Biliverdin reductase A deficiency reveals sex- and brain region-specific vulnerability to high-fat diet feeding

Simona Lanzillotta [a], Valeria Sommella [a], Barbara Zulli [a], Anna Picca [b,c], Riccardo Calvani [c,d], Sara Pagnotta [a], Gabriele Paolozzi [a], Mathilde Charlier [e], Emanuele Marzetti [c,d], Flavia Agata Cimini [f], Maria Gisella Cavallo [f], Bindu D. Paul [g,h,i], D. Allan Butterfield [j], Fabio Di Domenico [a], Marzia Perluigi [a], Antonella Tramutola [a], Eugenio Barone [a,*]

[a] Department of Biochemical Sciences "A. Rossi-Fanelli", Faculty of Pharmacy and Medicine, Sapienza University of Rome, Italy
[b] Department of Medicine and Surgery, LUM University, Casamassima, Italy
[c] Fondazione Policlinico Universitario "Agostino Gemelli" IRCCS, Rome, Italy
[d] Department of Geriatrics, Orthopedics and Rheumatology, Università Cattolica del Sacro Cuore, Rome, Italy
[e] Institute of Neuroscience, Group of Neuropharmacology, Université Catholique de Louvain, Avenue Hippocrate 53 (B1.53.01), Brussels, 1200, Belgium
[f] Department of Experimental Medicine, Sapienza University of Rome, Italy
[g] Department of Physiology, Pharmacology, & Therapeutics, Johns Hopkins University School of Medicine, Baltimore, MD, 21205, USA
[h] Department of Psychiatry and Behavioral Sciences, Johns Hopkins University School of Medicine, Baltimore, MD, 21205, USA
[i] The Solomon H. Snyder Department of Neuroscience, Johns Hopkins University School of Medicine, Baltimore, MD, 21205, USA
[j] Sanders-Brown Center on Aging, Department of Chemistry, University of Kentucky, Lexington, KY, 40506-0055, USA

ARTICLE INFO

Keywords:
Biliverdin reductase A
Redox homeostasis
Insulin signaling
Mitochondrial adaptation
Metabolic stress
Sex-differences

ABSTRACT

How the brain senses and responds to early metabolic stress, and why this process fails differently across sexes and regions, remains poorly understood. Here we show that biliverdin reductase A (BVRA) loss is associated with sex- and brain region-specific effects in response to high-fat diet (HFD) feeding, impairing insulin signaling and mitochondrial responses in selected brain regions while being associated with adaptive liver remodeling and improved systemic glucose handling in female mice. Using wild-type and whole-body BVRA-deficient mice of both sexes exposed to short-term high-fat diet (HFD) followed by dietary normalization, we show that BVRA loss is sufficient to induce cortical insulin resistance within just one week, phenocopying eight weeks of HFD and preceding detectable oxidative distress or mitochondrial failure. This sequence supports a model in which dysfunctional insulin signaling may represent an early event in the cascade of brain metabolic injury. The frontal cortex is the earliest and most vulnerable brain region, whereas the hippocampus shows delayed and milder alterations, suggesting brain region-specific vulnerability to HFD. Strikingly, F mice develop cognitive impairments indistinguishable from M mice despite substantially milder molecular alterations, revealing a sex-specific dissociation between molecular severity and functional outcome. After dietary normalization, M mice show partial recovery of cortical insulin signaling, mitochondrial function, and recognition memory. In contrast, F mice exhibit progressive BVRA decline, worsening insulin signaling uncoupling, and persistent cognitive deficits that outlast dietary exposure — revealing a metabolic memory encoded at the molecular level. These findings identify BVRA loss as a potential causal and sex-biased determinant of brain metabolic vulnerability, with implications for understanding the sex-differential susceptibility to insulin resistance-related neurodegeneration.

1. Introduction

Insulin resistance is a central metabolic alteration linking obesity, type 2 diabetes (T2D), and neurodegenerative disorders, including Alzheimer's disease (AD) [1,2]. Beyond its systemic metabolic consequences, impaired insulin signaling in the brain has emerged as a critical contributor to synaptic dysfunction, cognitive decline, and neurodegeneration, giving rise to the concept of "brain insulin resistance" as a

* Corresponding author.
E-mail address: eugenio.barone@uniroma1.it (E. Barone).

https://doi.org/10.1016/j.redox.2026.104404
Received 23 July 2026; Received in revised form 8 September 2026; Accepted 14 September 2026
Available online 18 September 2026

risk factor for neurodegeneration and dementia [1–7]. However, despite extensive investigation, the molecular determinants that define why specific tissues, brain regions, and sexes display different degrees of vulnerability to metabolic stress remain poorly understood. Accumulating evidence indicates that metabolic dysfunction does not affect the brain uniformly [8,9]. Cortical and hippocampal regions differ in energy demand, mitochondrial organization, and stress responsiveness [8,9], and these differences are further modulated by sex-specific metabolic and hormonal contexts [10]. Notably, while long-term high-fat diet (HFD) paradigms have been widely used to model insulin resistance and metabolic disease [11], far less is known about the earliest molecular events triggered by dietary stress in the brain and about how these early changes shape longer-lasting metabolic and cognitive outcomes. This gap in knowledge is particularly relevant given that metabolic insults in humans often occur intermittently or transiently yet may still seed persistent vulnerability.

Biliverdin reductase A (BVRA) has recently emerged as a pleiotropic metabolic regulator positioned at the intersection of insulin signaling, redox homeostasis, and mitochondrial function [12]. Originally characterized for its role in heme metabolism [12], BVRA is now recognized as an active signaling protein that modulates insulin receptor pathways [12–17], regulates oxidative and nitrosative stress [15,18–22], and influences mitochondrial dynamics and bioenergetic efficiency [15,23]. Reduced BVRA levels and activity have been reported in metabolic disorders, i.e., obesity [24,25], T2D [21,26], and AD [15,27,28], suggesting that BVRA loss may represent a convergent molecular event linking metabolic stress to neurodegenerative processes. Nevertheless, whether BVRA directly contributes to tissue-specific metabolic vulnerability, or instead reflects downstream adaptation to metabolic dysfunction, remains unresolved. Importantly, BVRA displays region- and tissue-specific expression patterns [18,19] and is subject to regulation by metabolic state [12,29,30], oxidative stress [18,30], and inflammation [30–32]. These properties raise the possibility that BVRA may contribute to a molecular buffering system that sets a threshold for metabolic resilience, thereby modulating how tissues adapt to metabolic challenge. In this context, short-term HFD exposure offers a powerful framework to dissect early adaptive versus maladaptive responses, allowing separation of primary vulnerability mechanisms from secondary consequences of prolonged metabolic disease.

Here, we investigated the role of BVRA in modulating, region-, and sex-specific responses to short-term dietary stress. Using wild-type and BVRA-deficient mice of both sexes exposed to a relatively short HFD, followed by dietary normalization, we systematically examined insulin signaling, redox balance, mitochondrial function, and cognitive performance across the frontal cortex (FC), hippocampus (HIP), and liver (LIV). This integrative approach allowed us to map a brain region-specific pattern of vulnerability and recovery to HFD, to assess how reduced BVRA protein levels alter the coupling between insulin signaling and mitochondrial adaptation, and whether BVRA-associated responses to HFD feeding were shared across central and peripheral tissues.

2. Methods

2.1. Mouse colonies

C57BL/6J mice were purchased from Charles River Laboratories. Biliverdin reductase A–deficient mice ($BVRA^{-/-}$) on a C57BL/6J background [19] were kindly provided by Dr. Bindu D. Paul (Johns Hopkins University) under Material Transfer Agreement #A38246. Mice were bred and maintained under specific pathogen-free (SPF) conditions at the animal facility located at the Department of Anatomical, Histological, Forensic Medicine and Orthopedics Sciences (SAIMLAL), Sapienza University of Rome. Animals were housed in clear Plexiglas cages (20 × 22 × 20 cm) under standard laboratory conditions with a temperature of 22 ± 2 ∘C and 70% humidity, a 12-h light/dark cycle, and ad libitum access to water and standard chow. All the experiments were performed in strict compliance with the Italian National Laws (DL 116/92), the European Communities Council Directives (86/609/EEC). Experimental protocol was approved by Italian Ministry of Health authorizations (#522/2020-PR and #426/2024-PR). All efforts were made to minimize the number of animals used in the study and their suffering.

2.2. Diet

C57BL/6J mice were chosen because they develop systemic and brain insulin resistance (but not diabetes) without a pronounced development of obesity and adiposity (which could represent confounding factors) once fed a HFD over 12 weeks, starting at 4 weeks of age [11]. Hence, at 4 weeks of age, male (M) and female (F) C57BL/6J and $BVRA^{-/-}$ mice were randomly assigned to receive either a purified control diet (13% kcal from fat; diet composition: protein 20%, fat 5%, fiber 4.7%, ash 6.1%, minerals 3.03%) thereafter standard diet (SD), or a purified HFD (60% kcal from fat; diet composition: protein 23.5%, fat 27.3%, carbohydrate 27.3%, minerals 4.8%) for either 1 week or 8 weeks. Furthermore, in a subset of C57BL/6J mice, dietary washout experiments were performed. In particular, after 8 weeks of HFD, mice were switched back to a SD for an additional 8 weeks (HFD8→SD8). M and F mice were group-housed (3–5 animals per cage), and maintained in separate cages with free access to water and food. Experimental groups were defined based on diets (SD or HFD), diet duration (1 week or 8 weeks), genotype (+/+ or −/−) and sex (M or F), and were housed separately (Table 1). In F mice, the estrous cycle was monitored throughout the dietary intervention. Diets were purchased from Mucedola srl, Italy. At the end of the dietary intervention, mice underwent a series of metabolic, behavioral, and molecular assessments (detailed below) and were subsequently sacrificed. Tissues were rapidly collected, snap-frozen in liquid nitrogen, and stored at −80 °C until further analysis.

2.3. Morphometric analyses

Body weight (g) and body length (cm) were measured in all mice at the beginning and at the end of the dietary intervention. Body mass index (BMI) was calculated as the ratio between body weight and body surface area (BSA, g/m^2). BSA was estimated using the DuBois formula [33] as follows:

$$\text{Body surface area } (m^2) = 0.007184 \times \text{weight } (kg)^{0.425} \times \text{body length } (cm)^{0.725}$$

Table 1
Experimental groups used in the project.

Diet	Genotype	Sex	Diet duration	ID
SD	C57BL/6J	M	1 week	$SD^{+/+}$1-M
SD	C57BL/6J	F	1 week	$SD^{+/+}$1-F
HFD	C57BL/6J	M	1 week	$HFD^{+/+}$1-M
HFD	C57BL/6J	F	1 week	$HFD^{+/+}$1-F
SD	C57BL/6J	M	8 weeks	$SD^{+/+}$8-M
SD	C57BL/6J	F	8 weeks	$SD^{+/+}$8-F
HFD	C57BL/6J	M	8 weeks	$HFD^{+/+}$8-M
HFD	C57BL/6J	F	8 weeks	$HFD^{+/+}$8-F
SD	$BVRA^{-/-}$	M	1 week	$SD^{-/-}$1-M
SD	$BVRA^{-/-}$	F	1 week	$SD^{-/-}$1-F
HFD	$BVRA^{-/-}$	M	1 week	$HFD^{-/-}$1-M
HFD	$BVRA^{-/-}$	F	1 week	$HFD^{-/-}$1-F
SD	$BVRA^{-/-}$	M	8 weeks	$SD^{-/-}$8-M
SD	$BVRA^{-/-}$	F	8 weeks	$SD^{-/-}$8-F
HFD	$BVRA^{-/-}$	M	8 weeks	$HFD^{-/-}$8-M
HFD	$BVRA^{-/-}$	F	8 weeks	$HFD^{-/-}$8-F
HFD8→SD8	C57BL/6J	M	8 weeks + 8 weeks	WO
HFD8→SD8	C57BL/6J	F	8 weeks + 8 weeks	WO

2.4. Intraperitoneal Glucose Tolerance Test (IPGTT)

Mice were fasted for 6 h prior to the IPGTT. Glucose was administered by intraperitoneal injection at a dose of 1.5 g/kg body weight. Blood glucose levels were measured from tail vein blood using a glucometer and test strips (CONTOUR® NEXT, Ascensia Diabetes Care Holdings AG, Basel, Switzerland). Glycemia was assessed at baseline (0 min) and at 30, 60, 90, and 120 min following glucose injection.

2.5. Behavioral tests

All behavioral assessments were performed during the light phase of the cycle by investigators blinded to genotype and dietary condition.

Novel Object Recognition (NOR): Recognition memory was evaluated using the NOR test, which exploits the innate tendency of rodents to preferentially explore novel objects over familiar ones. The task consisted of three sequential phases. On day 1 (habituation), each mouse was individually allowed to freely explore an empty open-field arena (50 cm length × 30 cm width × 30 cm height) for 10 min.

On day 2 (familiarization), mice were placed in the same arena containing two identical objects (two balls) and allowed to explore them for 5 min. To avoid forced interaction, animals were released facing the center of the opposite wall with their back toward the objects.

On day 3 (test phase), after a 24-h retention interval, mice were reintroduced into the arena containing one familiar object and one novel object (ball + plastic brick) and allowed to explore for 5 min. Exploration times were recorded and used to calculate: the Discrimination Index (DI) = (TN − TF)/(TN + TF), where TN and TF represent the time spent exploring the novel and familiar objects, respectively; and the Preference Index (PI) = TN/(TN + TF) × 100. A PI >50% indicated preference for the novel object, whereas values ≤ 50% reflected impaired recognition memory.

Y-maze test: Short-term spatial recognition memory and exploratory activity were assessed using the Y-maze spontaneous alternation task. The apparatus consisted of three identical arms (40 cm long × 8 cm high × 15 cm wide at the bottom and 10 cm at the top), positioned at 120° from each other and converging into a central triangular area (4 cm at its longest axis). The test consisted of two phases. During the training session, mice were placed at the end of one arm and allowed to explore the maze for 5 min, with one arm closed. After a 30-min inter-trial interval, animals underwent the testing session, in which they were reintroduced into the maze with all arms accessible and allowed to explore freely for 5 min. Entry into an arm was counted when all four paws entered an arm. The primary assessment parameters in this test are the time spent in the new arm and/or the number of times the animal entered it, which function as indicators of its spatial recognition and memory abilities. The *Preference Index* was calculated as: (the number of entries in the novel arm/total number of entries) × 100. In addition, the total number of arm movements was recorded as an indicator of locomotor activity, to ensure that any differences in the exploration of the new arm were not due to a change in overall activity.

2.6. Intranasal Insulin (INI) treatment

To assess acute brain insulin signaling responsiveness, a subset of mice from each experimental group was subjected to INI administration. Animals were fasted for 6 h prior to treatment to minimize variability in basal insulin signaling. Human insulin (Humalog®, KwikPen, Eli Lilly Nederland B.V.; ATC code A10AB04) was delivered intranasally at a total dose of 1 IU (10 μL/nostril) as previously described [15,34,35]. Control animals received an equivalent volume of vehicle (sterile saline solution). Intranasal delivery was performed by gently pipetting the solution onto each nostril, allowing spontaneous inhalation. Thirty minutes after INI or vehicle administration, mice were sacrificed, and brain tissues were rapidly dissected, snap-frozen in liquid nitrogen, and stored at −80 °C until biochemical analyses.

2.7. Sample preparation

Total protein extracts were obtained from the FC, HIP, and LIV of each experimental group. Tissues were homogenized in Tissue Protein Extraction Reagent (T-PER; Thermo Fisher Scientific, Waltham, MA, USA) supplemented with protease and phosphatase inhibitor cocktails (Sigma-Aldrich, St. Louis, MO, USA). Homogenization was performed using a Wheaton tissue homogenizer (45 strokes), followed by brief sonication to ensure complete lysis. Samples were then centrifuged at 14,000 rpm for 30 min at 4 °C to remove insoluble debris. The resulting supernatants were collected, and total protein concentration was determined using the bicinchoninic acid (BCA) assay according to the manufacturer's instructions (Thermo Fisher Scientific).

2.8. Western blot

Equal amounts of protein (15 μg) were resolved by sodium dodecyl sulfate–polyacrylamide gel electrophoresis (SDS–PAGE) using 4–15% gradient Criterion TGX Stain-Free precast gels (Bio-Rad, Hercules, CA, USA) in Tris/Glycine/SDS (TGS) running buffer (Bio-Rad Laboratories, #1610772). Immediately after electrophoresis, gels were UV-activated using a ChemiDoc MP imaging system (Bio-Rad Laboratories, #17001402) and Image Lab software (Bio-Rad) to acquire total protein load images. Proteins were then transferred onto nitrocellulose membranes using the Trans-Blot Turbo semi-dry transfer system (Bio-Rad Laboratories, #1704150). Membranes were blocked in Tris-buffered saline (TBS) containing 0.01% Tween-20 and 3% bovine serum albumin (SERVA Electrophoresis GmbH, Heidelberg, Germany) and incubated overnight at 4 °C with primary antibodies listed in Table 2. After washing, membranes were incubated for 1 h at room temperature with the appropriate horseradish peroxidase–conjugated secondary antibodies (Table 2). Immunoreactive bands were visualized using Clarity enhanced chemiluminescence (ECL) substrate (Bio-Rad Laboratories, #1705061) and acquired with the ChemiDoc MP imaging system. Densitometric analyses were performed using Image Lab 6.1 software (Bio-Rad Laboratories). Protein expression levels were normalized to total protein load using stain-free technology. This approach allows

Table 2
List of antibodies used in the project.

Antigen	Supplier	Host	Dilution
Primary antibody			
3-NT	R&D – MAB48	M	1:500
4-HNE	R&D – MAB3249	M	1:500
AKT	Cell Signaling - 9272S	R	1:1000
AMPK	Invitrogen – MA514922	M	1:1000
BVRA	Enzo – ADIOSA450E	R	1:1000
Complex I (NDUFB8)	Abcam – AB192878	R	1:5000
drp1	Cell Signaling - #14647	M	1:1000
GSK3β	Invitrogen – PA595845	R	1:1000
mTOR	Biolegend – 6H9B10	M	1:1000
NRF1	Invitrogen – MA532782	R	1:1000
P70S6K	Cell Signaling – 9202S	R	1:1000
PARKIN	Abcam - AB77924	M	1:1000
PGC1α	Proteintech – 663691ig	M	1:10000
phospho(S2448)-mTOR	Cell Signaling – 5536S	R	1:1000
phospho(S473)-AKT	Cell Signaling – 4060S	R	1:1000
phospho(S9)-GSK3β	Cell Signaling – 9336S	R	1:1000
phospho(T172)-AMPK	Cell Signaling – 2535S	R	1:1000
phospho(T389)-P70S6K	Cell Signaling – 9206S	M	1:1000
Protein Carbonyl	Sigma-Aldrich - S7150	R	1:5000
TFAM	Santa Cruz – sc166965	M	1:1000
Total OXPHOS	Abcam – Ab110413	M	1:3000
HRP-conjugated secondary antibodies:			
mouse IgG	Biorad - L005662		1:10000
rabbit IgG	Biorad - L005661		1:10000
Alkaline phosphatase-conjugated secondary antibodies:			
mouse IgG	Sigma-Aldrich - A3688		1:10000
rabbit IgG	Sigma-Aldrich - A9919		1:10000

accurate lane-to-lane normalization by quantifying the total protein signal and minimizes variability associated with reference proteins.

2.9. Slot blot analysis

To evaluate total protein-bound (i) 4-hydroxy-2-nonenal (4-HNE) and (ii) 3-nitrotyrosine (3-NT) levels, 5 μL of FC, HIP, and LIV protein homogenates were incubated with 10 μL of Laemmli buffer (0.125 M Tris base, pH 6.8, 4% (v/v) SDS, and 20% (v/v) glycerol) for 20 min at room temperature and then loaded onto nitrocellulose membranes as described below. For the detection of protein carbonyls (PC), 3 μL of FC, HIP, and LIV protein homogenates were first derivatized at room temperature for 20 min in 10 mM 2,4-dinitrophenylhydrazine (DNPH) and 5 μL of 12% sodium dodecyl sulfate (SDS). Samples were subsequently neutralized with 7.5 μL of neutralization solution (2 M Tris base in 30% glycerol). For all analyses, 250 ng of total protein were loaded per well onto nitrocellulose membranes under vacuum using a slot blot apparatus. Membranes were blocked for 1 h at room temperature with 3% bovine serum albumin (SERVA Electrophoresis GmbH, Heidelberg, Germany) in Tris-buffered saline (TBS) containing 0.01% Tween-20 and then incubated for 2 h at room temperature with the appropriate primary antibodies (anti-PC, anti-4-HNE or anti–3-NT; see Table 2). After three washes with TBS containing 0.01% Tween-20, membranes were incubated for 1 h at room temperature with the corresponding alkaline phosphatase–conjugated secondary antibodies (Table 2). Membranes were then washed three additional times and developed using Sigma Fast BCIP/NBT substrate (5-bromo-4-chloro-3-indolyl phosphate/nitro blue tetrazolium). Blots were air-dried, acquired using a ChemiDoc MP imaging system (Bio-Rad Laboratories, Hercules, CA, USA, #17001402), and analyzed with Image Lab software (version 6.0; Bio-Rad). No non-specific antibody binding to the membrane was detected. To allow comparison across samples processed on different slot blot membranes, two internal control samples were included on each membrane. These internal controls were loaded together with experimental samples in every slot blot run. Signal intensities were first normalized to the average of the internal control samples for each membrane, thereby correcting for inter-membrane variability. Subsequently, all normalized values were pooled and expressed relative to the mean value of the WT standard diet group at 1 week, which was set as reference.

2.10. BVRA ELISA assay

BVRA protein levels were quantified in FC, HIP, and LIV samples using a commercially available ELISA kit (Cat# LS-F74186, LifeSpan BioSciences, Seattle, WA, USA), following the manufacturer's instructions. Protein concentrations were determined prior to the assay, and equal amounts of total protein were loaded for each sample. BVRA levels were normalized to total protein content and expressed as ng of BVRA per μg of total protein.

2.11. PanY IRS1 ELISA assay

PanY of IRS1 in FC, HIP, and LIV samples were evaluated by an ELISA kit (PathScan® Phospho-IRS-1 (panTyr) Sandwich, Cat#7133, Cell Signaling Technology, Danvers, USA) according to the manufacturer's instructions. The amount of IRS1 Y phosphorylation was detected at 450 nm.

2.12. Electron Transport Chain (ETC) complexes enzymatic activity measurements

Mitochondrial complexes activities were measured in cryopreserved FC, HIP, and LIV samples, as previously described by Valenti et al. [36] with minor modifications. Tissue dissections were performed in ice-cold preservation buffer containing 50 mM K-MES (pH 7.1), 3 mM K_2HPO_4, 9.5 mM $MgCl_2$, and 3 mM ATP. Samples were then transferred to cryotubes containing the same buffer supplemented with 20% glycerol and 10 mg/mL fatty acid–free bovine serum albumin. Tissues were rapidly frozen in liquid isopentane to ensure uniform cryopreservation and maintained at −30 to −35 °C before long-term storage at −80 °C or on dry ice. For enzymatic assays, cryopreserved tissues were thawed on ice and the activities of mitochondrial Complex I, Complex II, and Complex IV measured using commercially available kits according to the manufacturer's instructions. For instance, Complex I Enzyme Activity Kit (ab109721), Complex II Enzyme Activity Kit (ab109908), and Cytochrome *c* Oxidase (Complex IV) Assay Kit (ab239711) (Abcam, Cambridge, UK).

2.13. Bio-plex assay

A magnetic bead–based immunoassay was used to measure levels of eight phosphoproteins pertaining to the insulin signaling pathway in the FC, HIP and LIV samples. All mediators were assayed in multiplex using the Bio-Plex ProCell Signaling protein kinase B (Akt) Panel, 8-plex (Bio-Rad Laboratories, #LQ00006JK0K0RR) to measure levels of the following phosphorylated proteins: insulin receptor substrate- 1 at S636 ($pIRS1^{Ser636}$), phosphatase and tensin homolog at S380 ($pPTEN^{S380}$), serine/threonine protein kinase Akt-1 at S473 ($pAKT^{S473}$), glycogen 47 synthase kinase- 3α/β at S21/S9 ($pGSK\text{-}3\alpha/\beta^{S9}$), mTOR at S2448 ($pmTOR^{S2448}$), p70 S6 kinase at T389 ($pP70S6K^{T389}$), ribosomal protein S6 kinase beta-1 at S235/236 ($pS6^{S235/S236}$), and the Bcl2-associated agonist of cell death at S136 ($pBAD^{S136}$). Experiments were run on a Bio-Plex System with Luminex xMAP Technology (Bio-Rad Laboratories) and data were acquired on a Bio-Plex Manager Software 6.1 (Bio-Rad Laboratories) with instrument default settings. Median fluorescence intensities (MFI) corrected for the blank background were obtained for all analytes and results were calculated as the ratio between the MFI of phosphorylated targets and total proteins.

2.14. Statistical analysis

Statistical analyses were performed using GraphPad Prism (version 10.0). Data are presented as mean ± SEM unless otherwise specified. Normality of data distribution was assessed using the Shapiro–Wilk test. Comparisons between two independent groups were performed using unpaired two-tailed Student's t-test. Comparisons among multiple groups were performed using analysis of variance (ANOVA), with the statistical model matched to the factorial structure available for each endpoint. For endpoints in which all combinations of diet (SD vs HFD), genotype (+/+ vs −/−), and diet duration were available, three-way ANOVA was applied to assess main effects and interaction terms. When missing values were present within otherwise factorially structured datasets, mixed-effects models fitted by restricted maximum likelihood (REML) were used to test the same main effects and interaction terms. For several molecular endpoints, however, the experimental design was intentionally not fully crossed but organized as a hypothesis-driven set of comparisons around a defined reference condition (see below), so that not all factorial cells were present. Under these conditions, endpoints were analyzed by one-way ANOVA followed by Dunnett's post hoc test. The hypothesis-driven one-way ANOVA/Dunnett analyses are reported in Supplementary Table 1–6, whereas the additional factorial analyses are reported in Supplementary Tables 7–10. Given that the reduction of BVRA protein levels represented the primary biological hypothesis of the study, the statistical analyses were performed accordingly. BVRA expression levels were first analyzed by one-way ANOVA to identify the dietary condition associated with a significant reduction in BVRA. This analysis demonstrated that BVRA levels were selectively reduced after 8 weeks of HFD, but not after 1 week of HFD or under SD. Based on these results, the HFD 8-week condition ($HFD^{+}/^{+}8$) was defined as the reference group for subsequent analyses. Accordingly, for insulin-signaling, mitochondrial, and redox-related endpoints, comparisons were primarily performed using one-

way ANOVA followed by Dunnett's post hoc test, comparing all experimental groups to $HFD^{+}/^{+}8$. This approach allowed assessment of whether BVRA reduction was associated with specific molecular alterations and whether BVRA-deficient mice phenocopied the changes observed in WT mice under HFD. To further evaluate whether BVRA loss was sufficient to induce these alterations, additional one-way ANOVA analyses were conducted comparing WT and $BVRA^{-/-}$ mice at early time points (SD and HFD, 1 week). These analyses were designed to determine whether BVRA deficiency alone was able to reproduce molecular features otherwise observed only after prolonged dietary stress. Correlations between continuous variables were assessed using Pearson's correlation coefficient. Values were standardized by z-score transformation separately for each sex and region, using the mean and standard deviation calculated from the corresponding pooled group ($z = [x - \text{mean}]/SD$). z-score standardization was restricted to the WT groups in which BVRA is expressed and shows a graded reduction (HFD1 and HFD8), since the aim was to test whether variation in BVRA levels is associated with changes in insulin-signaling readouts. A p value < 0.05 was considered statistically significant. For each figure panel, the specific statistical test applied, and the number of biological replicates is reported in the figure legends.

3. Results

3.1. Peripheral metabolic alterations associated with BVRA loss under HFD

To characterize the systemic metabolic state associated with BVRA deficiency and HFD exposure, we first examined body weight, BMI, BSA, and fasting glucose in WT mice fed with SD ($SD^{+/+}$) or HFD ($HFD^{+/+}$) and $BVRA^{-/-}$ mice following the same diet regimen (thereafter, $SD^{-/-}$ and $HFD^{-/-}$) for 1 and 8 weeks [37]. WT and $BVRA^{-/-}$ mice did not differ in terms of body weight, BMI, or BSA at the beginning of the dietary intervention (T0). Short-term HFD did not alter body weight, BMI, or BSA in WT or $BVRA^{-/-}$ mice of either sex at one or eight weeks, except for a modest BSA increase in $BVRA^{-/-}$ F mice at 8 weeks (Fig. 1A–F). Fasting glucose was similarly unaffected by genotype or diet across groups. HFD impaired glucose tolerance in M mice at both timepoints, as measured by the IPGTT area under the curve (AUC), independently of BVRA genotype (Fig. 1G–L). In F mice, HFD likewise impaired glucose tolerance in WT animals; however, $BVRA^{-/-}$ F mice were protected from this effect, maintaining AUC values comparable to SD-fed WT mice under both 1- and 8-weeks HFD (Fig. 1M–R). BVRA deficiency was associated with a sex-specific systemic glucose phenotype, in which HFD-induced glucose intolerance was not observed in $BVRA^{-/-}$ F mice.

3.2. Metabolic stress promotes a reduction of BVRA in a sex- and region-dependent manner

To determine whether HFD promotes a reduction of BVRA protein levels as observed in humans [25], we evaluated levels of BVRA in the FC, HIP and LIV of $SD^{+/+}$ or $HFD^{+/+}$ and $BVRA^{-/-}$ mice ($SD^{-/-}$ and $HFD^{-/-}$) after 1 and 8 weeks of diet (Fig. 2A). BVRA was undetectable in $BVRA^{-/-}$ mice confirming the validity of the genetic model (Fig. 2B). $HFD^{+/+}$ mice exhibited a significant decrease of BVRA protein levels in both the brain and in the LIV after 8 weeks of diet, with sex-dependent differences (Fig. 2C–D). BVRA protein levels were significantly reduced as function of both diet (SD *vs* HFD) and diet exposure (1-week HFD *vs* 8-weeks HFD) in the FC of $HFD^{+/+}$8-M and $HFD^{+/+}$8-F mice (Fig. 2C and D). A significant reduction was also observed in the HIP of $HFD^{+/+}$8-M mice (Fig. 2C), whereas no changes were detected in the HIP of $HFD^{+/+}$8-F mice (Fig. 2D). In parallel, lower BVRA protein levels only in the LIV of $HFD^{+/+}$8-F mice, were observed (Fig. 2D). Notably, basal BVRA abundance differed across tissues in a sex-dependent pattern: in M mice, BVRA was highest in the LIV relative to FC and HIP; in F mice, both HIP and LIV showed higher basal BVRA than the FC (Fig. 2C–D). This tissue-specific gradient of basal BVRA abundance is consistent with the differences we observed between the FC and the HIP and with the LIV ability to cope with HFD-induced metabolic stress described in subsequent sections.

3.3. Loss of BVRA triggers the development of insulin resistance in the FC of M mice under HFD

To assess whether BVRA deficiency is associated with early alterations in brain insulin-signaling response and whether this mechanism is relevant to the development of cell metabolism alterations, we first evaluated the basal activation of key components of the insulin pathway in the FC of WT and $BVRA^{-/-}$ mice (Fig. 3A–J). These analyses were performed using an ELISA assay to quantify $panIRS1^{Y}$ levels along a multiplex approach, which allows the simultaneous quantification of multiple phospho-targets, i.e., $pIRS1^{S636}$, $pPTEN^{S380}$, $pAKT^{S473}$, $pGSK3\beta^{S9}$, $pmTOR^{S2448}$, $pP70S6K^{T389}$, and $pS6^{S235/S236}$, $pBAD^{S136}$. $HFD^{+/+}$8-M mice, show a marked increase of IRS1 inhibition ($pIRS1^{S636}$) (Fig. 3B). Downstream from IRS1, a significant increase of AKT activation ($pAKT^{S473}$, Fig. 3D) along with a consistent modulation of AKT targets including the inhibition of GSK3β ($pGSK3\beta^{S9}$, Fig. 3E), the hyper-activation of the mTOR ($pmTOR^{S2448}$, Fig. 3F) and the activation of BAD ($pBAD^{S136}$, Fig. 3G), were observed. Activation of P70S6K ($pP70S6K^{T389}$) did not show significant change (Fig. 3H), while its downstream target S6 protein was found significantly activated ($pS6^{S235/S236}$, Fig. 3I). This pattern is consistent with established markers of brain insulin resistance [1,3,34]. Remarkably, $BVRA^{-/-}$ M mice recapitulated this full signaling signature after only one week of HFD ($HFD^{-/-}$1-M), phenocopying the molecular profile of $HFD^{+/+}$8-M (Fig. 3A–I). In addition, several signaling differences were already evident in $SD^{-/-}$1-M mice. Both PTEN inhibition ($pPTEN^{S380}$) (Fig. 3C) and $pP70S6K^{T389}$ (Fig. 3H) levels were significantly reduced in $SD^{-/-}$1-M compared to $SD^{+/+}$1-M, suggesting that the absence of BVRA alters the basal insulin signaling tone and primes the system for an aberrant response to metabolic stress. The reduction of BVRA protein levels in the $HFD^{+/+}$ group ($HFD^{+/+}1 \rightarrow HFD^{+/+}8$) showed strong negative correlations with multiple components of the insulin signaling cascade, including AKT, GSK3β, and the mTOR–S6 axis (Fig. 3K–L), consistent with BVRA abundance setting the dynamic range of cortical insulin responsiveness. Furthermore, and in agreement with previous data [15,38], $BVRA^{-/-}$ mice show no changes for $pGSK3\beta^{S9}$ (Fig. 3E) despite increased AKT activation. The experimental design also included $BVRA^{-/-}$ mice exposed to both SD and HFD for 8 weeks, enabling systematic comparison across genotypes, diets, and timepoints. Eight-week BVRA−/− data confirmed a signaling profile distinct from $HFD^{+/+}$8-M and are presented in Supplementary Table 1A. Factorial analysis further supported an endpoint-specific remodeling of cortical insulin signaling in M mice, involving genotype, diet, diet duration, and selected interaction terms, consistent with the interpretation that BVRA deficiency modifies the temporal response of the pathway to metabolic stress (Supplementary Table 7A).

3.4. Acute insulin responsiveness is impaired in the FC of M mice fed with HFD

To test whether basal signaling alterations translated into defective acute insulin responsiveness, we administered intranasal insulin (INI) to WT and $BVRA^{-/-}$ mice and we evaluated pathway activation by looking at key targets, i.e., $panIRS1^{Y}$, AKT, GSK3β, mTOR and P70S6K (Fig. 4A–J). Based on the results described above, we compared $HFD^{+/+}$8-M mice with $BVRA^{-/-}$ mice after 1 week of diet (both $SD^{-/-}$1-M and $HFD^{-/-}$1-M). These conditions were the most informative for mechanistic analyses unraveling how brain insulin resistance develops. $SD^{+/+}$8-M mice were included as the normometabolic reference. In $SD^{+/+}$8-M mice, INI treatment did not increase $panIRS1^{Y}$ levels after 30 min

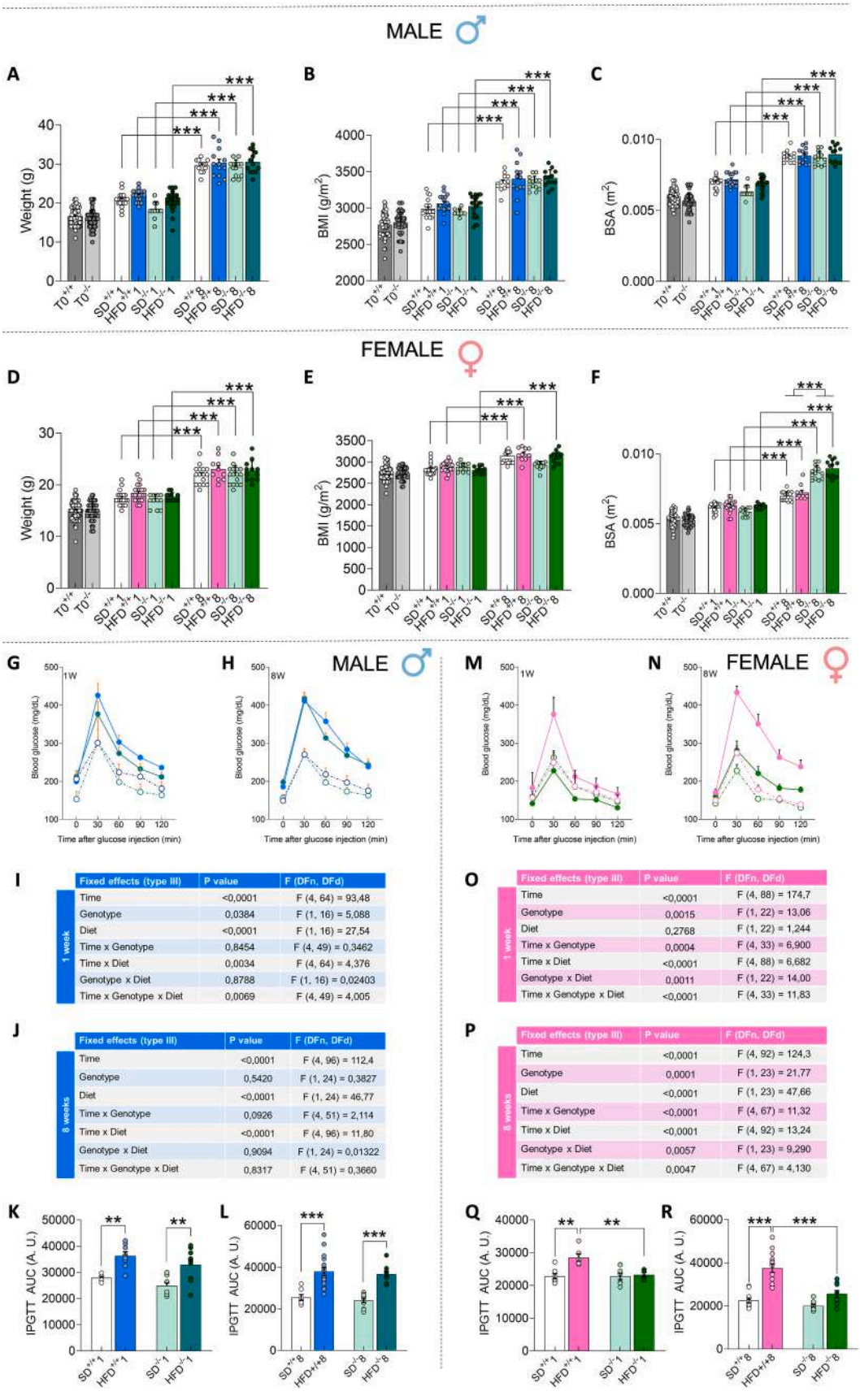

I	Fixed effects (type III)	P value	F (DFn, DFd)
1 week	Time	<0,0001	F (4, 64) = 93,48
	Genotype	0,0384	F (1, 16) = 5,088
	Diet	<0,0001	F (1, 16) = 27,54
	Time x Genotype	0,8454	F (4, 49) = 0,3462
	Time x Diet	0,0034	F (4, 64) = 4,376
	Genotype x Diet	0,8788	F (1, 16) = 0,02403
	Time x Genotype x Diet	0,0069	F (4, 49) = 4,005

J	Fixed effects (type III)	P value	F (DFn, DFd)
8 weeks	Time	<0,0001	F (4, 96) = 112,4
	Genotype	0,5420	F (1, 24) = 0,3827
	Diet	<0,0001	F (1, 24) = 46,77
	Time x Genotype	0,0926	F (4, 51) = 2,114
	Time x Diet	<0,0001	F (4, 96) = 11,80
	Genotype x Diet	0,9094	F (1, 24) = 0,01322
	Time x Genotype x Diet	0,8317	F (4, 51) = 0,3660

O	Fixed effects (type III)	P value	F (DFn, DFd)
1 week	Time	<0,0001	F (4, 88) = 174,7
	Genotype	0,0015	F (1, 22) = 13,06
	Diet	0,2768	F (1, 22) = 1,244
	Time x Genotype	0,0004	F (4, 33) = 6,900
	Time x Diet	<0,0001	F (4, 88) = 6,682
	Genotype x Diet	0,0011	F (1, 22) = 14,00
	Time x Genotype x Diet	<0,0001	F (4, 33) = 11,83

P	Fixed effects (type III)	P value	F (DFn, DFd)
8 weeks	Time	<0,0001	F (4, 92) = 124,3
	Genotype	0,0001	F (1, 23) = 21,77
	Diet	<0,0001	F (1, 23) = 47,66
	Time x Genotype	<0,0001	F (4, 67) = 11,32
	Time x Diet	<0,0001	F (4, 92) = 13,24
	Genotype x Diet	0,0057	F (1, 23) = 9,290
	Time x Genotype x Diet	0,0047	F (4, 67) = 4,130

(caption on next page)

Fig. 1. Peripheral metabolic alterations associated with BVRA loss under HFD.
(A and D) Body weight (g), (B and E) body mass index (BMI, g/m^2), and (C and F) body surface area (BSA, m^2) evaluated in WT and BVRA$^{-/-}$ mice (M and F) at the beginning of the diet (T0) and after 1 week or 8 weeks of either SD or HFD. n = 10-23 mice/group. One-way ANOVA with Bonferroni *post-hoc* test. **p < 0.01, ***p < 0.001
(G) Intraperitoneal glucose tolerance test (IPGTT) performed in male WT or BVRA$^{-/-}$ mice after 1 week of either SD or HFD. n = 7-9 mice/group.
(H) Intraperitoneal glucose tolerance test (IPGTT) performed in male WT or BVRA$^{-/-}$ mice after 8 weeks of either SD or HFD. n = 7-16 mice/group.
(I) Results of the Three-way ANOVA relative to the IPGTT performed in male WT or BVRA$^{-/-}$ mice after 1 week of either SD or HFD.
(J) Results of the Three-way ANOVA relative to the IPGTT performed in male WT or BVRA$^{-/-}$ mice after 8 weeks of either SD or HFD.
(K) Area Under Curve (AUC) relative to the IPGTT performed in male WT or BVRA$^{-/-}$ mice after 1 week of either SD or HFD. n = 7-9 mice/group. One-way ANOVA with Bonferroni *post-hoc* test. **p < 0.01, ***p < 0.001
(L) Area Under Curve (AUC) relative to the IPGTT performed in male WT or BVRA$^{-/-}$ mice after 8 weeks of either SD or HFD. n = 7-16 mice/group. One-way ANOVA with Bonferroni *post-hoc* test. **p < 0.01, ***p < 0.001
(M) Intraperitoneal glucose tolerance test (IPGTT) performed in female WT or BVRA$^{-/-}$ mice after 1 week of either SD or HFD. n = 5-8 mice/group.
(N) Intraperitoneal glucose tolerance test (IPGTT) performed in female WT or BVRA$^{-/-}$ mice after 8 weeks of either SD or HFD. n = 9-14 mice/group.
(O) Three-way ANOVA relative to the IPGTT performed in female WT or BVRA$^{-/-}$ mice after 1 week of either SD or HFD.
(P) Three-way ANOVA relative to the IPGTT performed in female WT or BVRA$^{-/-}$ mice after 8 weeks of either SD or HFD.
(Q) Area Under Curve (AUC) relative to the IPGTT performed in female WT or BVRA$^{-/-}$ mice after 1 week of either SD or HFD. n = 5-8 mice/group. One-way ANOVA with Bonferroni *post-hoc* test. **p < 0.01, ***p < 0.001
Area Under Curve (AUC) relative to the IPGTT performed in female WT or BVRA$^{-/-}$ mice after 8 weeks of either SD or HFD. n = 9-14 mice/group. One-way ANOVA with Bonferroni *post-hoc* test. **p < 0.01, ***p < 0.001.

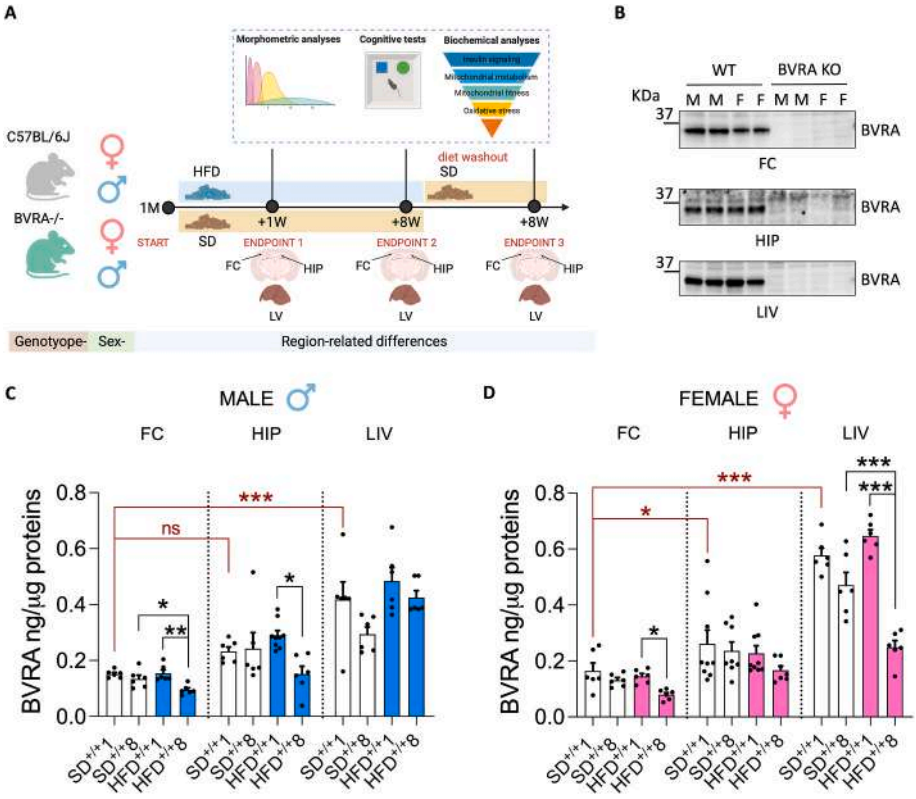

Fig. 2. HFD promotes BVRA loss in a region- and sex-dependent manner.
(A) Schematic representation of the study design
(B) Representative western blotting images of BVRA protein levels evaluated in the frontal cortex (FC), hippocampus (HIP) and liver (LIV) of wild-type mice (C57BL/6J$^{+/+}$) and BVRA deficient mice (C57BL/6J$^{-/-}$) of both sex (M and F).
(C) BVRA protein levels evaluated in the frontal cortex (FC), hippocampus (HIP) and liver (LIV) of M mice fed with SD or HFD for either 1 week or 8 weeks. n = 6-9 mice/group.
(D) BVRA protein levels evaluated in the frontal cortex (FC), hippocampus (HIP) and liver (LIV) of F mice fed with SD or HFD for either 1 week or 8 weeks. n = 6-9 mice/group.
Data presented as mean ± SEM. Differences were tested separately for each region (in black). Differences in basal BVRA levels (in red) were also tested across different regions and tissues. One-way ANOVA with Bonferroni *post-hoc* test. *p < 0.05, ***p < 0.001.

(Fig. 4A, F, and 4G). However, INI significantly activated AKT (Fig. 4B, F, and 4G) and mTOR (Fig. 4D, F, and 4G) suggesting a functional transduction of the insulin signaling, likely due to earlier IRS1 activation peaking before 30 min [15,29,34,35,39,40]. In contrast, HFD$^{+/+}$8-M mice failed to respond to INI, showing no IRS1 activation and no modulation of downstream signaling, indicating impaired cortical insulin sensitivity after dietary stress (Fig. 4A–G). Notably, INI administration in HFD$^{+/+}$8-M mice induced a further significant reduction of BVRA protein levels (Fig. 4H and I). This observation suggests that, under conditions of metabolic stress, acute insulin stimulation elicits

downregulation of BVRA, potentially serving as a compensatory attempt to enhance insulin signaling sensibilization at the level of IRS1 [12]. However, despite this further reduction, downstream pathway activation remained defective, indicating that acute BVRA loss is insufficient to restore coordinated insulin signal propagation. In line with this, $SD^{-/-}$1-M mice showed partial responsiveness to INI, with increased $panIRS1^{Y}$ levels and AKT activation, without significant differences observed for the other targets (Fig. 4A–G), consistent with the proposed role for BVRA [12]. Strikingly, $HFD^{-/-}$1-M mice showed a dysregulated response to INI, closely mimicking what observed in $HFD^{+/+}$8-M mice: no changes for $panIRS1^{Y}$ and AKT activation, but abnormally increased GSK3β inhibition and mTOR activation, along with reduced P70S6K activation (Fig. 4A–G). In addition, $BVRA^{-/-}$ mice stimulated with INI after 8 weeks of SD or HFD show a profoundly aberrant signaling response with sustained phosphorylation of multiple targets at levels markedly higher than those observed in WT mice (Supplementary Fig. 1A–E). Together, these findings establish that BVRA depletion — whether genetic or diet-induced — abolishes acute cortical insulin

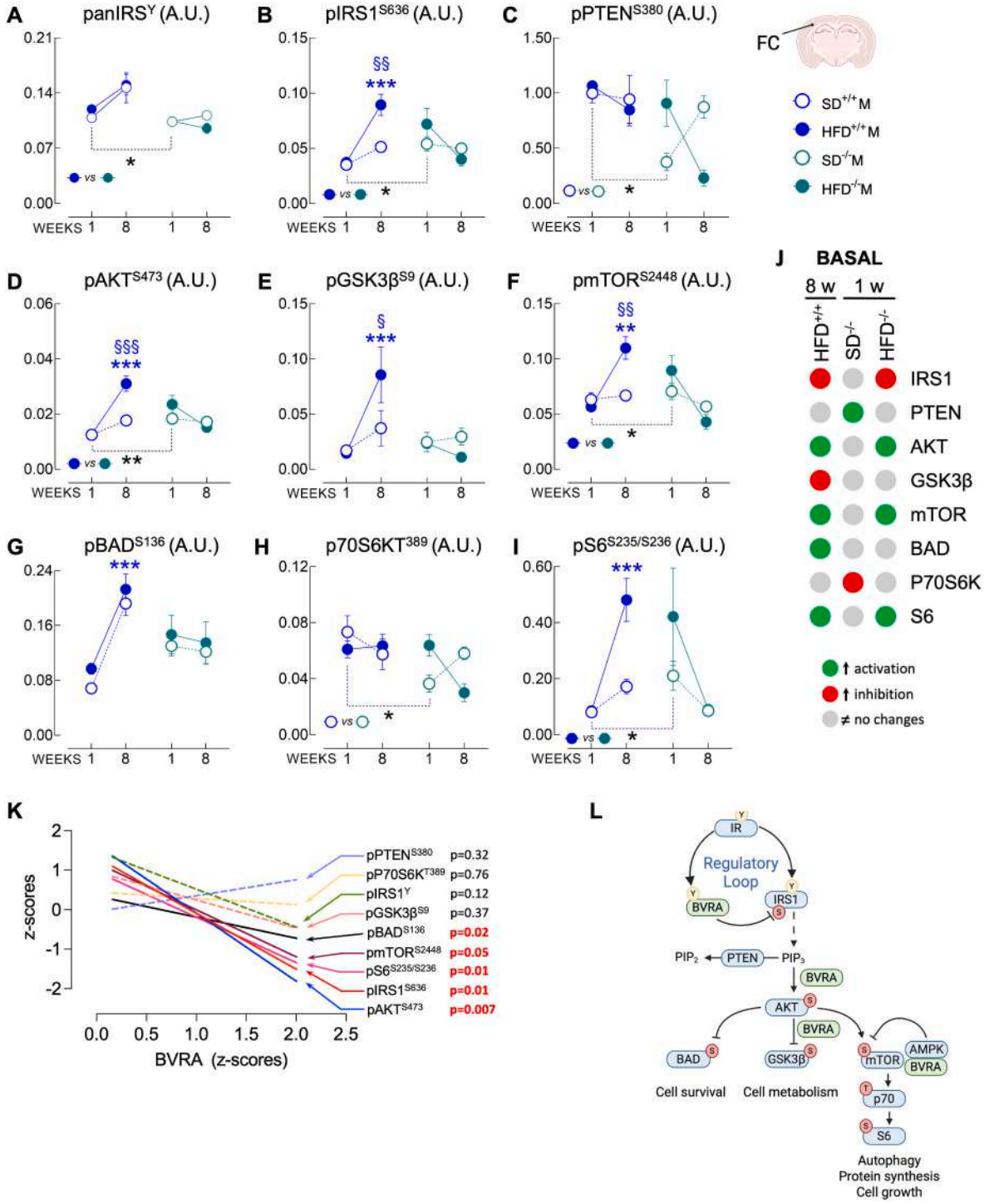

(caption on next page)

Fig. 3. Loss of BVRA triggers the development of insulin resistance in the FC of M mice
(A-I) Levels of proteins of the insulin signaling evaluated in the FC of WT and BVRA$^{-/-}$ M mice fed with SD or HFD for either 1 week or 8 weeks. n = 6 mice/group. Data presented as mean ± SEM. One-way ANOVA with Dunnett's post-hoc test using the HFD$^{+/+}$8 group as reference. *p < 0.05, **p < 0.01, ***p < 0.001 vs HFD$^{+/+}$1; §p < 0.05, §§p < 0.01, §§§p < 0.001 vs SD$^{+/+}$8. 'To test whether BVRA deficiency in BVRA$^{-/-}$ mice phenocopies changes observed in WT mice fed with HFD for 8 weeks a further one-way ANOVA followed by Bonferroni post-hoc test was performed comparing WT and BVRA$^{-/-}$ mice at early time points (SD and HFD, 1 week). Groups found significantly different were highlighted by the relative legend. *p < 0.05, **p < 0.01.
(J) Schematic representations reporting the activation (green), inhibition (red) or no changes (grey) of the proteins of the insulin signaling in WT mice fed with HFD for 8 weeks and BVRA$^{-/-}$ mice fed with SD or HFD for 1 week.
(K) Pearson correlations between BVRA protein levels and proteins of the insulin signaling evaluated in the FC of WT M mice fed with HFD for either 1 week or 8 weeks. Significant correlations are reported in red. p values are shown.
(L) Schematic representation of the insulin signaling with highlighted key points known to be regulated by BVRA as established by previous studies [see Tramutola A et al., Trends Endocrinol Metab 2026]. Upon insulin binding, the insulin receptor (IR) autophosphorylates on Y residues, activating its kinase activity and phosphorylating the insulin receptor substrate-1 (IRS1) on Y sites. IR also phosphorylates BVRA, which then acts as a S/T/Y kinase, phosphorylating IRS1 on inhibitory S residues as part of a regulatory loop that limits excessive IRS1 activation. Once activated, IRS1 promotes the activation of AKT (pAKT^{S473}) axis, which regulates glucose uptake via GLUT4 translocation and modulates key metabolic nodes including: (i) the inhibition of GSK3β (pGSK3β^{S9}) that contribute to cell metabolism, (ii) the inhibition of BAD (pBAD^{S136}) that prevents apoptosis and favors cell survival, and (iii) the activation of the mTOR axis (pmTOR^{S2448}/pP70S6K^{T389}/pS6$^{S235/S236}$), that regulates autophagy, protein synthesis and cell survival. Activation of insulin signaling downstream from IRS1 is also regulated by phosphatase PTEN which converts PIP3 in PIP2 thus preventing AKT activation. PTEN is inhibited once phosphorylated at S380 (pPTEN^{S380}).

responsiveness in M mice and that HFD$^{-/-}$1-M phenocopy the full molecular signature of established brain insulin resistance in HFD$^{+/+}$8-M mice.

3.5. BVRA deficiency is sufficient to induce insulin resistance in the FC of F mice

We analyzed the same signaling components in the FC of F mice (Fig. 5A–J). Unlike M mice, 8-weeks of HFD did not induce classical IRS1 inhibition in the FC of F mice, as no significant increase of pIRS1^{S636}, was observed (Fig. 5B). HFD produced milder but consistent alterations downstream from IRS1 compared to M mice, including increased levels of pAKT^{S473} (Fig. 5D), pGSK3β^{S9} (Fig. 5E), pmTOR^{S2448} (Fig. 5F), and pS6$^{S235/S236}$ (Fig. 5I) along with reduced pPTEN^{S380} levels (Fig. 5C). This pattern indicates that cortical insulin alterations are at an earlier and less penetrant stage in F mice, lacking the prominent IRS1 inhibition that characterizes the male response. Similar alterations were evident in SD$^{-/-}$1-F mice (Fig. 5A–I) suggesting that loss of BVRA is sufficient to trigger such changes in the absence of metabolic stress. SD$^{-/-}$1-F mice also showed a robust increase in pGSK3β^{S9} without proportional pAKT^{S473} elevation (Fig. 5E), consistent with an AKT-independent mechanism of GSK3β dysregulation distinct from the canonical BVRA-AKT-GSK3β axis previously reported [41]. Correlation analysis revealed that BVRA levels were significantly associated only with PTEN inhibitory phosphorylation in HFD$^{+/+}$8-F mice (Fig. 5K). This selective association aligns with the hypothesis that BVRA loss might act as a priming event that predisposes the pathway to post-receptor insulin resistance, even before overt downstream alterations. Also in F mice, chronic BVRA deficiency promoted a significant impairment of the basal insulin signaling pathway after 8 weeks of SD or HFD (Supplementary Table 1B). Factorial analysis further supported that BVRA deficiency is sufficient to promote specific remodeling of cortical insulin signaling in F mice, mainly affecting downstream pathway nodes rather than inducing a prominent IRS1 inhibition (Supplementary Table 7B).

3.6. Loss of BVRA is sufficient to impair acute insulin responsiveness in the FC of F mice

The hypothesized vulnerability of insulin signaling in the FC of F mice fed with HFD became even more evident upon INI administration. As observed in SD$^{+/+}$8-M mice, no changes for panIRS1^{Y} levels were found (Fig. 6A). INI elicited a significant physiological response characterized by the increase of AKT (Fig. 6B, F and 6G) and mTOR activation (Fig. 6D, F and 6G), along with reduced GSK3β inhibition in SD$^{+/+}$8-F mice (Fig. 6C, F and 6G). In striking contrast, INI failed to promote insulin signaling activation in the FC of HFD$^{+/+}$8-F (Fig. 6A–G). This defective response was accompanied by a further acute reduction of BVRA levels (Fig. 6H–I), mirroring the male HFD response. Notably, the impaired response to acute insulin occurred in the absence of increased pIRS1^{S636} levels at baseline, demonstrating that functional insulin resistance in female FC can be established independently of canonical IRS1 inhibition and due to reduced BVRA. In agreement, the effects produced by the INI administration to SD$^{-/-}$1-F mice closely resembled to those observed in HFD$^{+/+}$8-F mice (Fig. 6A–G). This impairment persists in HFD$^{-/-}$1-F mice (Fig. 6A–G). BVRA$^{-/-}$ mice stimulated with INI after 8 weeks of SD or HFD show a profoundly aberrant signaling response (Supplementary Fig. 2) as for male, thus reinforcing the role for chronic BVRA loss.

These findings support a model in which loss of BVRA represents a critical and sufficient determinant of insulin resistance development in the female brain, even in the absence of canonical IRS1 inhibition.

3.7. Cortical insulin resistance precedes oxidative distress

To establish the temporal relationship between dysfunctional insulin signaling and oxidative distress, we quantified three established oxidative distress markers [27,42–45], i.e., 4-HNE, 3-NT, PC, in the FC of M and F mice. In WT animals, neither sex showed significant changes in oxidative distress markers following 8 weeks of HFD (Fig. 7A–F), indicating that a relatively short dietary stress was not sufficient to induce oxidative distress in the FC. This temporal dissociation — insulin signaling dysfunction preceding oxidative stress — positions brain insulin resistance as an early consequence of BVRA reduction rather than a downstream effect of oxidative injury. Conversely, BVRA$^{-/-}$ mice exhibited a marked increase of the measured markers. In M mice, 4-HNE were elevated regardless of diet, while 3-NT and PC levels were significantly increased only in response to HFD (Fig. 7A, C, and 7E, Supplementary Table 2A). In F mice all the three markers were elevated regardless of diet (Fig. 7B, D, and 7F, Supplementary Table 2B), suggesting a greater susceptibility to oxidative damage, in agreement with the insulin signaling alterations. Factorial analysis further supported that FC oxidative distress was predominantly associated with BVRA deficiency, with marker- and sex-specific interaction patterns rather than a uniform diet-driven oxidative response (Supplementary Table 7A–B). The increase in oxidative distress marker levels observed in BVRA$^{-/-}$ mice was consistent with our prior studies, which showed that genetic depletion of BVRA perturbs redox balance [18,19].

Given that BVRA levels were decreased only in WT mice after 8 weeks of HFD, and the alterations in insulin signaling closely resembled those detected in BVRA$^{-/-}$ mice already after just 1 week of either SD or HFD in a sex-dependent manner, we conducted all subsequent analyses on these specific groups. This approach facilitated identification the earliest molecular changes associated with BVRA deficiency, while minimizing the confounding effects of long-term dietary exposure.

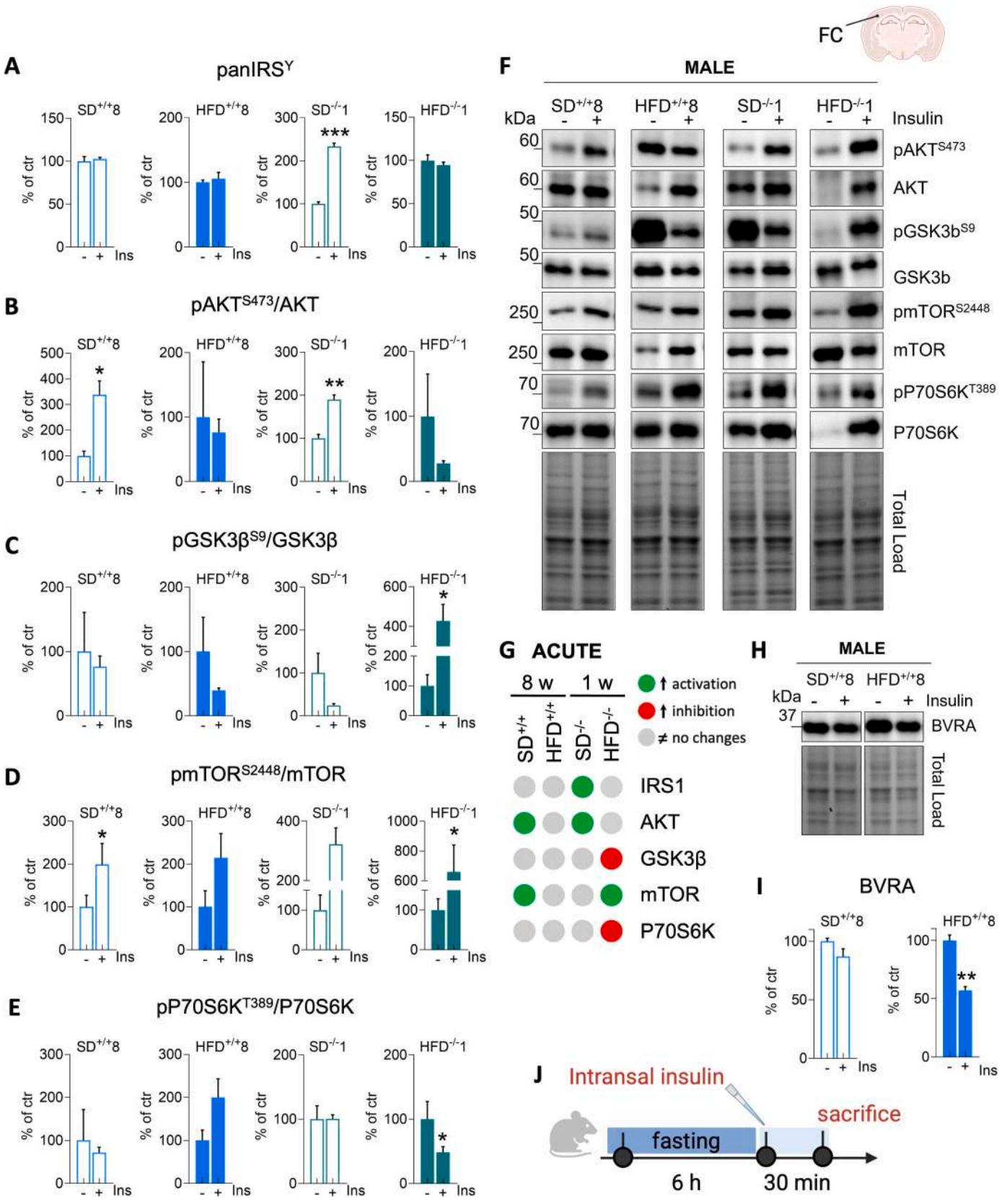

(caption on next page)

Fig. 4. Acute insulin responsiveness is impaired in the FC of M mice fed with HFD
(A-E) Activation of proteins of the insulin signaling pathway evaluated in the FC of WT M mice fed with HFD for 1 or 8 weeks and BVRA$^{-/-}$ M mice fed with SD or HFD for 1 week. IRS1 activation was evaluated as pIRS1^{Y} levels; AKT activation was evaluated as pAKT^{S473}/AKT ratio; GSK3β inhibition was evaluated as pGSK3β^{S9}/GSK3β ratio; mTOR activation was evaluated as pmTOR^{S2448}/mTOR ratio; and P70S6K activation was evaluated as pP70S6K^{T389}/P70S6K ratio. n = 3 mice/group. Values are given as percentage of vehicle set as 100%. Data presented as mean ± SEM. Student *t*-test: *p < 0.05, **p < 0.01, **p < 0.001. (−) vehicle; (+): insulin 1IU.
(F) Representative western blotting images of the proteins presented in B-E.
(G) Schematic representations reporting the activation (green), inhibition (red) or no changes (grey) of the proteins of the insulin signaling evaluated in the FC of WT mice fed with HFD for 1 or 8 weeks and BVRA$^{-/-}$ M mice fed with SD or HFD for 1 week, and treated with intranasal insulin. n = 3 mice/group.
(H-I) Representative Western blot and densitometric evaluation of BVRA protein levels in the FC of WT mice fed with HFD for 1 or 8 weeks and treated with intranasal insulin. Values are given as percentage of vehicle set as 100%. Data presented as mean ± SEM. Student *t*-test: *p < 0.05, **p < 0.01, ***p < 0.001. (−) vehicle; (+): insulin 1IU. Densitometric analysis refers to the vehicle-versus-insulin comparison within each condition; the BVRA immunoblots are not intended for quantitative comparison of basal BVRA levels across groups.
(J) Schematic representation of the protocol used for the intranasal insulin administration.

3.8. Loss of BVRA is associated with mitochondrial adaptation in the FC of M mice under metabolic stress

Insulin resistance impairs mitochondrial function, particularly in brain regions enriched with insulin receptors and critically involved in memory processing [15,46–49], resulting in alterations of the ETC activity [15,46–49]. To investigate the impact of insulin resistance and BVRA deficiency on mitochondrial function, we assessed the expression and activity of mitochondrial complexes, as well key regulators of mitochondrial fitness, in the FC.

In HFD$^{+/+}$8-M a significant reduction in the expression of several OXPHOS subunits, i.e., CI, CII, CIII, and CIV, was observed, while CV levels remained unchanged (Fig. 8A–F). This pattern was closely mirrored in BVRA$^{-/-}$ mice already after 1 week of SD or HFD, confirming that BVRA deficiency is sufficient to induce mitochondrial remodeling. CV levels were significantly reduced only in HFD$^{-/-}$1-M mice (Fig. 8A–F), suggesting that stronger conditions, such as the combination of BVRA deficiency (or a major decrease, if we look at WT mice) and dietary stress, are required. Despite the reduction in structural components, enzymatic activities of CI, CII, and CIV were preserved in HFD$^{+/+}$8-M mice, and even increased in BVRA$^{-/-}$ mice at 1 week, regardless of diet (Fig. 8G–I), revealing a dissociation between structural and functional mitochondrial integrity. To identify the regulatory mechanism underlying this compensation, we measured key markers of mitochondrial fitness. Active AMPK form, as measured by phosphorylation at T172 (pAMPK^{T172}), was preserved in both WT and BVRA$^{-/-}$ mice regardless of diet, even in the presence of reduced total AMPK levels (Fig. 8J-L). In contrast, PGC1α was reduced in HFD$^{-/-}$1-M mice only, while NRF1 and TFAM were unchanged across all groups (Fig. 8J and 8M-O), dissociating AMPK activation from the canonical transcriptional biogenesis program [50,51]. DRP1 protein was elevated in HFD$^{+/+}$8-M and BVRA$^{-/-}$ mice (Fig. 8J and P), while PARKIN was unchanged (Fig. 8J and Q), likely suggesting activation of mitochondrial fission without concurrent mitophagy. Mitochondrial fragmentation reflects an adaptive quality-control response, whereby damaged mitochondria are segregated, yet the remaining network becomes functionally hyperactive to sustain energetic demand [51–53]. Together, these data propose AMPK-driven DRP1-dependent mitochondrial fission, independent from both transcriptional biogenesis and mitophagic clearance, as a potential adaptive mechanism sustaining ETC function in male FC during the early phase of BVRA depletion-induced metabolic stress.

3.9. Mitochondrial adaptation fails in the FC of F mice under metabolic stress

In the FC of HFD$^{+/+}$8-F mice a broad reduction in ETC subunits was observed, as for M mice. CII and CIII were significantly decreased (Fig. 9A–F), while CI and CV showed a near-significant reduction (Fig. 9A–F), a pattern also observed in BVRA$^{-/-}$ mice (Fig. 9A–F), that reflects a downstream consequence of BVRA loss. In contrast to M mice, this structural remodeling was not accompanied by functional compensation (Fig. 9G–I). CI activity was increased (Fig. 9G), but CIV activity was significantly reduced in both HFD$^{+/+}$8-F and BVRA$^{-/-}$ mice (Fig. 9I), indicating compromised OXPHOS functionality at a terminal control node of the ETC.

Phosphorylation of AMPK was significantly increased in both HFD$^{+/+}$8-F and SD$^{-/-}$1-F (Fig. 9J–L), despite no changes for total AMPK levels (Fig. 9J–L). However, no significant differences were observed in the expression of PGC1α, TFAM, or NRF1 in HFD$^{+/+}$8-F and SD$^{-/-}$1-F (Fig. 9J and 9M-O), confirming that AMPK activation is dissociated from transcriptional biogenesis in both sexes. Elevated DRP1 without parallel PARKIN induction was similarly observed in HFD$^{+/+}$8-F and BVRA$^{-/-}$ mice (Fig. 9J and 9P-Q), likely suggesting that fission is engaged without concurrent mitophagy. Unlike in M mice, in F mice this fission response was accompanied by progressive CIV failure. Furthermore, the more pronounced deficits observed in HFD$^{-/-}$1-F mice relative to HFD$^{+/+}$8-F reflect the additive burden of genetic BVRA absence combined with dietary challenge.

3.10. Higher basal BVRA levels confer HIP resilience, while BVRA deficiency unmasks sex-specific vulnerabilities

To determine whether the metabolic alterations identified in the FC extend to the HIP, we performed parallel analyses across insulin signaling, mitochondrial function, and oxidative stress markers. Full data are presented in Supplementary Fig. 3–11 and Supplementary Tables 3–4, and 8A-8B; key findings are summarized here.

The HIP showed substantially greater resilience to short-term metabolic stress than the FC, with alterations emerging later and with lower penetrance, a pattern consistent with its higher basal BVRA abundance (Fig. 2C). In WT M mice, 8 weeks of HFD produced only mild basal insulin signaling alterations, characterized by reduced pIRS1^{S636} and the hyper-activation of downstream nodes (Supplementary Fig. 3, and Supplementary Table 3A–B). INI administration revealed a latent post-receptor defect: preserved IRS1 engagement with impaired AKT-mTOR propagation and further acute BVRA reduction (Supplementary Fig. 4–5). Mitochondrial adaptation was effective in M mice, with preserved OXPHOS subunit expression and increased CIV activity consistent with AMPK-dependent compensation in the absence of fission or biogenesis program activation (Supplementary Fig. 6). This profile is distinct from the DRP1-driven remodeling observed in the FC. BVRA deficiency accelerated the onset of both insulin signaling and mitochondrial alterations in BVRA$^{-/-}$ M mice, recapitulating the HFD$^{+/+}$8-M hippocampal phenotype at earlier timepoints (Supplementary Fig. 3–6) and reinforcing a possible role of BVRA as a factor associated with the threshold for HIP metabolic resilience. In F mice, HIP responses to HFD were even more attenuated: no significant basal changes in insulin signaling or mitochondrial function were detected in HFD$^{+/+}$8-F mice (Supplementary Fig. 7–10, Table 3B), consistent with the absence of HFD-induced BVRA reduction in F mice HIP (Fig. 2D). However, INI revealed a latent vulnerability characterized by the preserved IRS1 activation with failure to engage downstream effectors and

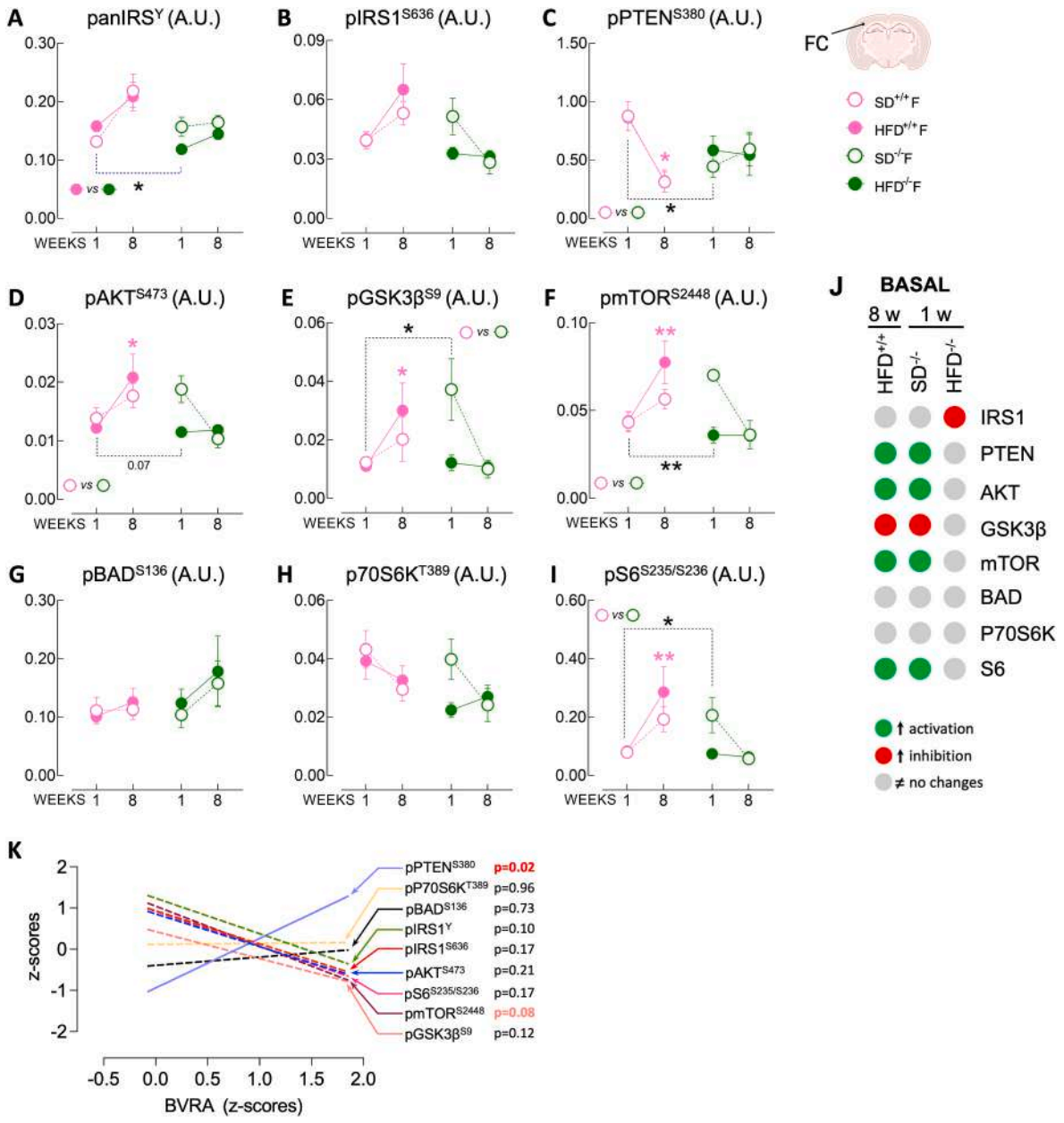

Fig. 5. Loss of BVRA is sufficient to promote the development of insulin resistance in the FC of F mice

(A-I) Levels of proteins of the insulin signaling evaluated in the FC of WT and BVRA$^{-/-}$ F mice fed with SD or HFD for either 1 week or 8 weeks. n = 6 mice/group. Data presented as mean ± SEM. One-way ANOVA with Dunnett's post-hoc test using the HFD$^{+/+}$8 group as reference. *p < 0.05, **p < 0.01, ***p < 0.001 vs HFD$^{+/+}$1; §p < 0.05, §§p < 0.01, §§§p < 0.001 vs SD$^{+/+}$8. To support the hypothesis that BVRA deficiency in BVRA$^{-/-}$ mice phenocopies changes observed in WT mice fed with HFD for 8 weeks a further one-way ANOVA followed by Bonferroni post-hoc test was performed comparing WT and BVRA$^{-/-}$ mice at early time points (SD and HFD, 1 week). Groups found significantly different were highlighted by the relative legend. *p < 0.05, **p < 0.01.

(J) Schematic representations reporting the activation (green), inhibition (red) or no changes (grey) of the proteins of the insulin signaling in WT mice fed with HFD for 8 weeks and BVRA$^{-/-}$ mice fed with SD or HFD for 1 week.

(K) Pearson correlations between BVRA protein levels and proteins of the insulin signaling evaluated in the FC of WT F mice fed with HFD for either 1 week or 8 weeks. Significant correlations are reported in red. P values are shown.

acute BVRA reduction (Supplementary Fig. 8–9). These results indicate that functional insulin resistance can be unmasked in F mice HIP despite the absence of basal molecular alterations. BVRA deficiency was sufficient to expose this vulnerability under SD, and one week of HFD further worsened the acute response (Supplementary Fig. 8–9). Mitochondrial defects, including reduced CIV activity and impaired mitophagy, were restricted to BVRA$^{-/-}$ F mice (Supplementary Fig. 10), revealing a BVRA-dependent mitochondrial fragility that HFD alone is insufficient to trigger in F mice at this timepoint. In both sexes, HIP insulin signaling and mitochondrial alterations occurred without widespread oxidative stress in WT mice under HFD, with only a mild increase in 4-HNE in HFD$^{+/+}$8-M mice (Supplementary Fig. 11, Table 4), replicating the temporal dissociation observed in the FC. BVRA deficiency selectively induced nitrosative stress (elevated 3-NT) accompanied by a paradoxical reduction in 4-HNE and PC levels in both sexes (Supplementary Fig. 11, Table 4), consistent with activation of compensatory antioxidant mechanisms at this earlier stage of hippocampal vulnerability [15].

Together, these findings point to a hierarchical sequence of metabolic vulnerability whereby HIP is impacted later than FC. Furthermore, while metabolic stress alters both basal and acute signaling in M mice, it

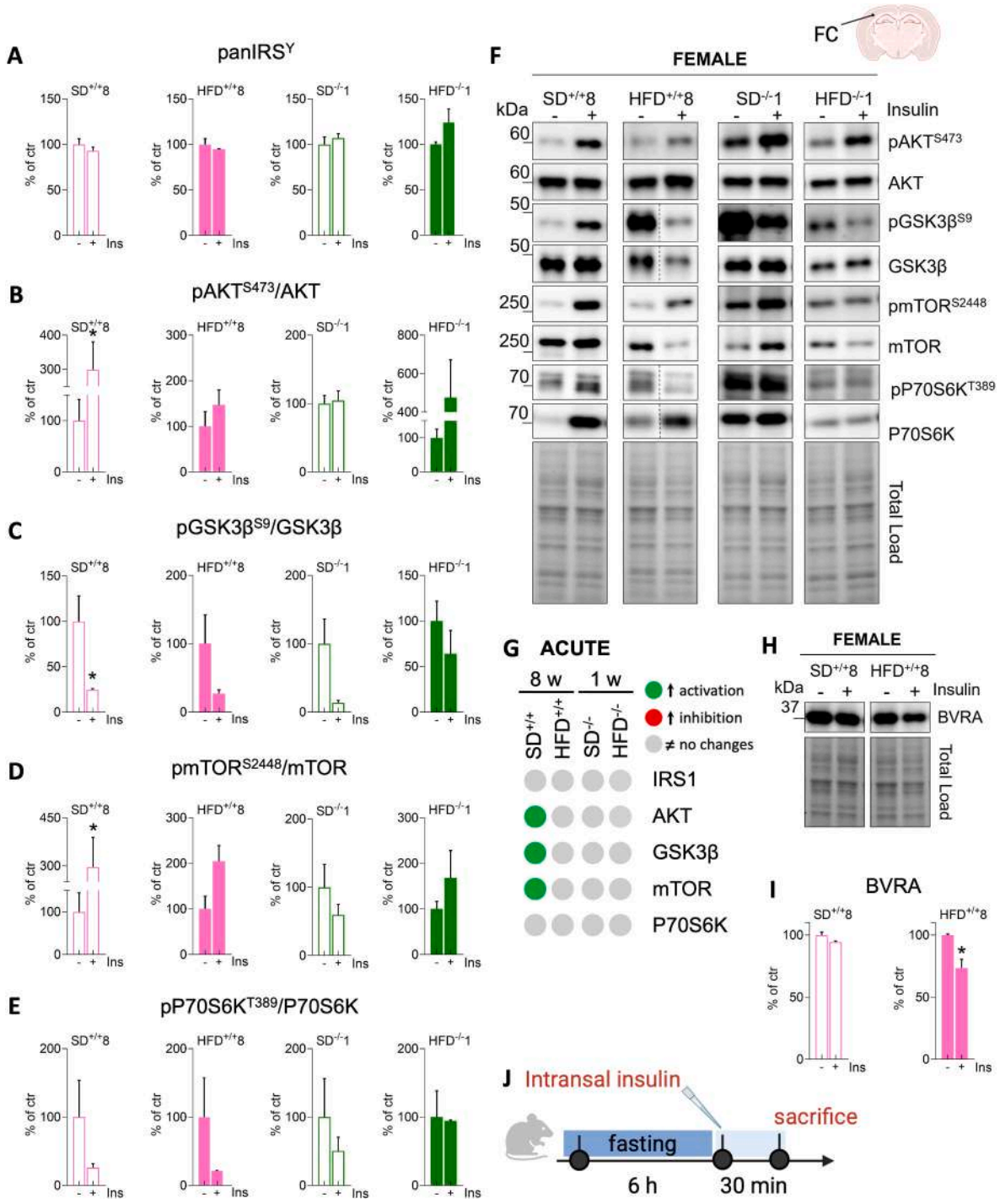

Fig. 6. Acute insulin responsiveness is impaired in the FC of F mice fed with HFD

(A-E) Activation of proteins of the insulin signaling pathway evaluated in the FC of WT F mice fed with HFD for 1 or 8 weeks and BVRA$^{-/-}$ F mice fed with SD or HFD for 1 week. IRS1 activation was evaluated as pIRS1^{Y} levels; AKT activation was evaluated as pAKT^{S473}/AKT ratio; GSK3β inhibition was evaluated as pGSK3β^{S9}/GSK3β ratio; mTOR activation was evaluated as pmTOR^{S2448}/mTOR ratio; and P70S6K activation was evaluated as pP70S6K^{T389}/P70S6K ratio. n = 3 mice/group. Values are given as percentage of vehicle set as 100%. Data presented as mean ± SEM. Student *t*-test: *p < 0.05, **p < 0.01, **p < 0.001. (−) vehicle; (+): insulin 1IU.

(F) Representative western blotting images of the proteins presented in B-E.

(G) Schematic representations reporting the activation (green), inhibition (red) or no changes (grey) of the proteins of the insulin signaling evaluated in the FC of WT mice fed with HFD for 1 or 8 weeks and BVRA$^{-/-}$ F mice fed with SD or HFD for 1 week and treated with intranasal insulin. n = 3 mice/group.

(H-I) Representative Western blot and densitometric evaluation of BVRA protein levels in the FC of WT mice fed with HFD for 1 or 8 weeks and treated with intranasal insulin. Values are given as percentage of vehicle set as 100%. Data presented as mean ± SEM. Student *t*-test: *p < 0.05, **p < 0.01, ***p < 0.001. (−) vehicle; (+): insulin 1IU. Densitometric analysis refers to the vehicle-versus-insulin comparison within each condition; the BVRA immunoblots are not intended for quantitative comparison of basal BVRA levels across groups.

(J) Schematic representation of the protocol used for the intranasal insulin administration.

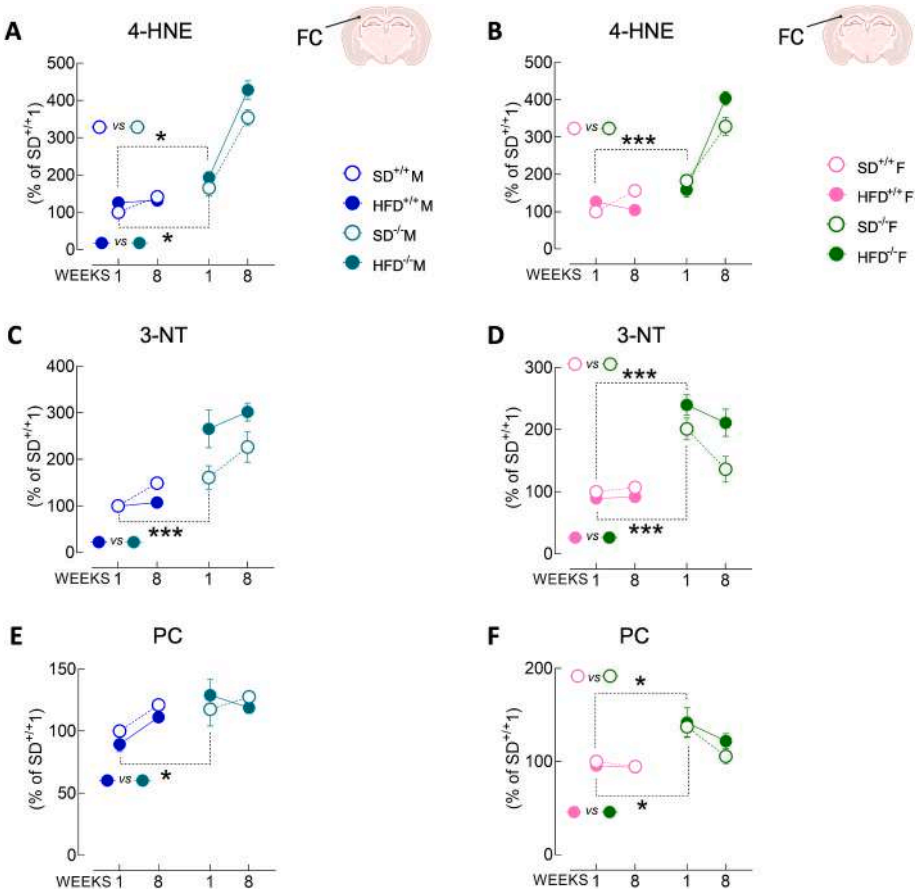

Fig. 7. Oxidative distress marker levels in the FC of M and F mice

(A, C, E) Densitometric analysis of the oxidative distress markers, i.e., protein-bound 4-hydroxy-2-nonenals (4-HNE), 3-nitrotyrosine (3-NT) and, protein carbonyls (PC), evaluated in the FC of WT and BVRA$^{-/-}$ M mice fed with SD or HFD for either 1 week or 8 weeks. n = 7 mice/group.

(B, D, F) Levels of the oxidative distress markers in the FC of WT and BVRA$^{-/-}$ F mice fed with SD or HFD for either 1 week or 8 weeks. n = 7 mice/group.

Data presented as mean ± SEM. One-way ANOVA with Dunnett's post-hoc test using the HFD$^{+/+}$8 group as reference. *p < 0.05, **p < 0.01, ***p < 0.001 vs HFD$^{+/+}$1; §p < 0.05, §§p < 0.01, §§§p < 0.001 vs SD$^{+/+}$8. To test the hypothesis that BVRA deficiency in BVRA$^{-/-}$ mice phenocopies changes observed in WT mice fed with HFD for 8 weeks a further one-way ANOVA followed by Bonferroni post-hoc test was performed comparing WT and BVRA$^{-/-}$ mice at early time points (SD and HFD, 1 week). Groups found significantly different were highlighted by the relative legend. *p < 0.05, **p < 0.01.

preferentially disrupts acute insulin responsiveness in F mice. In both sexes, BVRA deficiency accelerate the onset of insulin signaling and mitochondrial dysfunctions, anticipating alterations that would otherwise emerge with a prolonged metabolic stress and chronically reduced BVRA levels.

3.11. *The LIV displays adaptive remodeling under HFD*

To determine whether the metabolic alterations identified in the brain extend to a peripheral insulin-sensitive tissue, we performed parallel analyses in the LIV. Full data are presented in Supplementary Figs. 12–16, Supplementary Tables 5-6 and 9A-9B; key findings are summarized here.

The LIV showed greater resilience to short-term metabolic stress induced by HFD than either brain region, consistent with its higher basal BVRA abundance and with the high adaptive metabolic plasticity of the LIV. Thus, within the present short-term HFD paradigm, reduced BVRA does not translate into overt hepatic insulin resistance or worsened systemic glucose handling (Fig. 2C–D). In HFD$^{+/+}$8-M mice only mild and non-canonical alterations of hepatic insulin signaling were observed. These changes were characterized by reduced IRS1 inhibitory phosphorylation, together with preserved AKT activation and selective uncoupling of downstream nodes, i.e., increased GSK3β and mTOR phosphorylation in the absence of P70S6K and S6 engagement (Supplementary Fig. 12A–K, and Supplementary Table 5). These observations are consistent with a rewiring of hepatic insulin signaling rather than overt pathway inhibition [54,55]. At the mitochondrial level, M mice LIV exhibited a modest remodeling. OXPHOS subunit expression was largely preserved (Supplementary Fig. 13A–I), while a reduction in CIV activity emerged in HFD$^{+/+}$8-M mice (Supplementary Fig. 13I), consistent with selective remodeling of respiratory complex activity. No coordinated activation of mitochondrial biogenesis or quality-control pathways was observed (Supplementary Fig. 13J–Q). BVRA$^{-/-}$ M mice did not recapitulate these HFD-induced alterations, consistent with the absence of BVRA reduction in M mice LIV (Fig. 2C). The primary effect of BVRA deficiency was an abnormal reduction of CI and CIV activities together with alterations in proteins associated with both fission and mitophagy processes (Supplementary Fig. 13A–Q). Hence, BVRA deficiency might be associated with hepatic mitochondrial remodeling even in the absence of overt insulin resistance. In HFD$^{+/+}$8-F mice, the hepatic response followed a distinct trajectory. Despite a significant reduction of BVRA protein levels (Fig. 2D), insulin signaling remained largely preserved, with no evidence of IRS1 inhibition or downstream pathway alterations (Supplementary Fig. 14A–K, and Supplementary Table 6), indicating that partial BVRA reduction is functionally buffered by the high basal BVRA pool in the LIV and might represent an adaptive mechanism to HFD-induced stress (Fig. 2C). Hepatic mitochondrial complexes showed selective changes that account

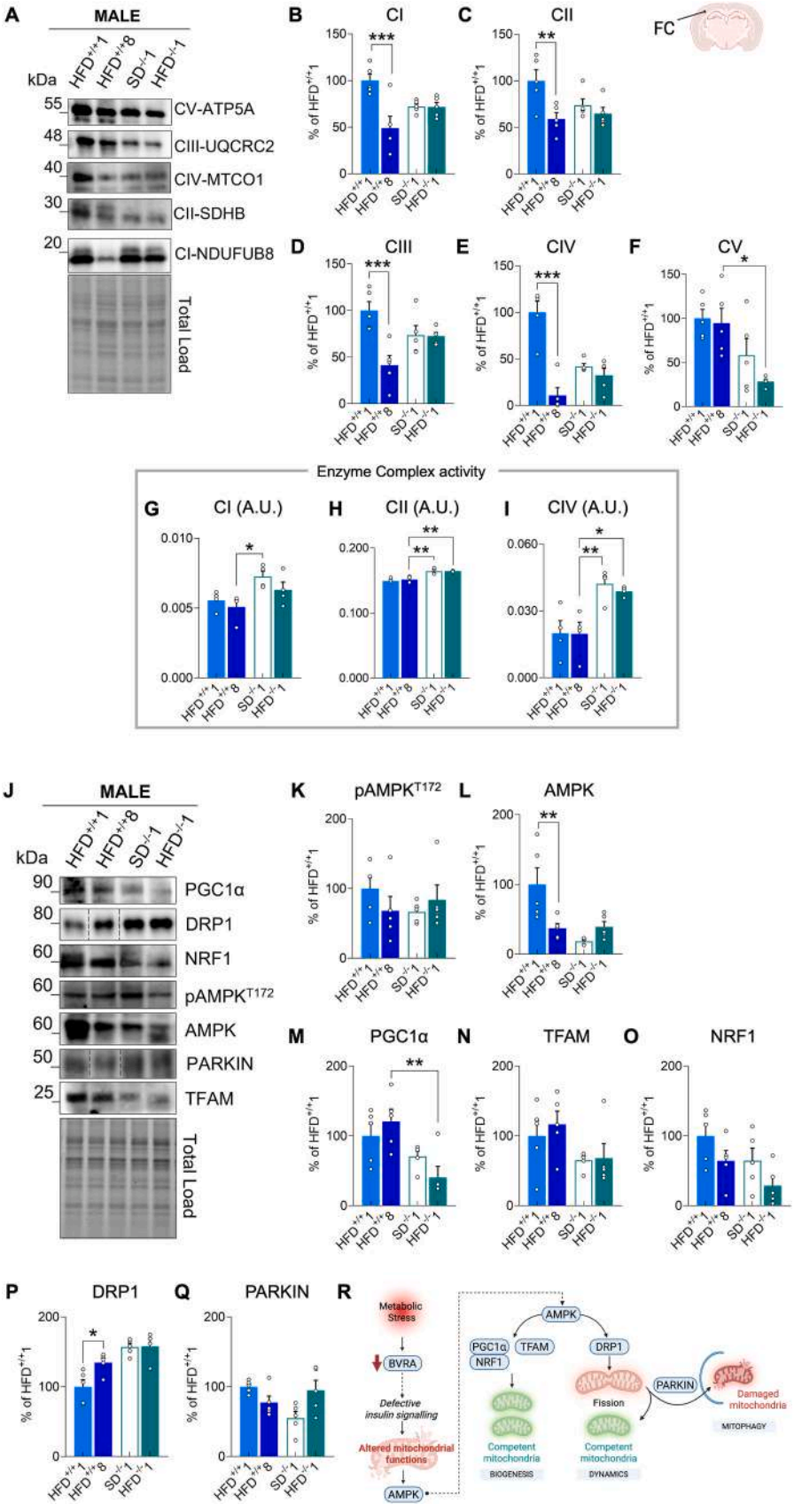

(caption on next page)

Fig. 8. Loss of BVRA promotes mitochondrial adaptation in the FC of M mice under metabolic stress
(A-F) Representative Western blot images and densitometric analysis of mitochondrial OXPHOS complexes subunits, i.e., CI (subunit NDUFB8), **C**II (subunit SDHB), **C**III (subunit UQCRC2), **C**IV (subunit MTCO1), **C**V (subunit ATP5A) evaluated in the FC of WT M mice fed with HFD for 1 or 8 weeks and BVRA$^{-/-}$ M mice fed with SD or HFD for 1 week. n = 5 mice/group. Values are given as percentage of WT fed with HFD for 1 week set as 100%. Data are presented as means ± SEM. One-way ANOVA with Dunnett's post-hoc test using the HFD$^{+/+}$8 group as reference. *p < 0.05, **p < 0.01, ***p < 0.001.
(G-I) Mitochondrial OXPHOS complexes activity evaluated in the FC of WT M mice fed with HFD for 1 or 8 weeks and BVRA$^{-/-}$ M mice fed with SD or HFD for 1 week. n = 3-4 mice/group. Data are presented as means ± SEM. One-way ANOVA with Dunnett's post-hoc test using the HFD$^{+/+}$8 group as reference. *p < 0.05, **p < 0.01, ***p < 0.001.
(J-Q) Representative Western blot images and densitometric analysis of proteins regulating mitochondrial fitness including, pAMPK^{T172}, total AMPK, PGC1α, TFAM, NRF1, DRP1 and PARKIN levels, evaluated in the FC of WT and BVRA$^{-/-}$ M mice fed with HFD for 1 or 8 weeks and BVRA$^{-/-}$ M mice fed with SD or HFD for 1 week. n = 5 mice/group Values are given as percentage of WT fed with HFD for 1 week set as 100%. Data are presented as means ± SEM. One-way ANOVA with Dunnett's post-hoc test using the HFD$^{+/+}$8 group as reference. *p < 0.05, **p < 0.01.
(R) Schematic model summarizing the observed associations between loss of BVRA, altered insulin signaling, and the mitochondrial response, integrated with existing literature. The scheme is not intended to imply a demonstrated causal or sequential dependency.

for a remodeling in response to HFD feeding: despite preserved ETC expression levels (Supplementary Fig. 15A–F), CI and CIV activities were significantly reduced (Supplementary Fig. 15G–I). These changes were accompanied by the activation of a transcriptional biogenetic program (increased TFAM, preserved AMPK) without coordinated engagement of proteins known to be involved in the regulation of fission or mitophagy processes (Supplementary Fig. 15J–Q). BVRA$^{-/-}$ F mice exhibited an attenuation of selected insulin signaling proteins activation together with reduced respiratory complex activities (Supplementary Figs. 14 and 15), suggesting that BVRA deficiency might lead to remodeling of hepatic insulin signaling and mitochondrial related parameters. In both sexes, HFD did not promote oxidative stress accumulation in the LIV, consistent with its greater redox resilience compared to brain (Supplementary Fig. 16).

Hence, the LIV displays a higher degree of metabolic resilience and adaptation compared to the brain, under HFD, with selected mitochondrial remodeling occurring without evidence of overt hepatic insulin resistance.

3.12. F mice show reduced cognitive resilience with respect to M mice under metabolic stress

Given the marked sex- and region-specific molecular differences observed across cortical and hippocampal circuits, we next evaluated whether HFD and BVRA deficiency translated into cognitive impairments. Long-term recognition memory (NOR, Fig. 10A–E) and short-term spatial working memory (Y-maze, Fig. 10F–J) were assessed after 1 or 8 weeks of diet. In M mice, HFD induced an early and progressive decline in NOR performance, with both PI and DI significantly reduced after 8 weeks (Fig. 10B–C). Notably, BVRA$^{-/-}$ M mice displayed comparable impairments regardless of diet, mirroring the phenotype of HFD$^{+/+}$8-M mice and supporting the concept that BVRA loss sensitizes cortical and hippocampal circuits to early cognitive dysfunction. Female mice exhibited a distinct vulnerability pattern. In WT F mice, NOR performance failed to show the age-dependent improvement observed under SD, and HFD$^{+/+}$8-F mice performed significantly worse than SD$^{+/+}$8-F mice (Fig. 10D–E). Strikingly, BVRA$^{-/-}$ F mice displayed comparable impairments even under SD (Fig. 10D–E). Importantly, these deficits emerged despite considerably milder molecular alterations than those observed in M mice, revealing reduced cognitive resilience of the female brain to metabolic stress. Factorial analyses further supported a BVRA genotype-related contribution to cognitive performance, particularly for NOR endpoints (Supplementary Table 10A–B).

Outcome of the Y-maze test did not differ significantly between HFD and SD groups in either sex (Fig. 10F–J), indicating preserved working memory under these conditions. However, BVRA$^{-/-}$ M mice showed reduced total arm entries (Fig. 10H), suggesting diminished exploratory drive or locomotor activity, possibly reflecting broader motivational or subcortical metabolic effects of BVRA deficiency. No locomotor differences were observed in F mice (Fig. 10J).

3.13. Effects of HFD outlast diet exposure in F mice

To determine whether HFD-induced defects were reversible, WT mice exposed to 8 weeks of HFD were returned to a standard diet for additional 8 weeks (HFD8→SD8, thereafter WO) and compared with the HFD8 condition. This paradigm was designed to model metabolic recovery following a defined period of dietary insult, conceptually analogous to the human scenario of weight gain on an obesogenic diet followed by return to a healthier diet; accordingly, the washout group was compared with its own pre-recovery condition (HFD8) to isolate the effect of dietary normalization on a background of established diet-induced dysfunction. In both sexes, the WO phase did not substantially modify anthropometric parameters (body weight, BMI and BSA), the subsequent metabolic and cognitive changes were not attributable to gross differences in body composition (Fig. 11A–C; 11G–I). Despite this, glucose handling markedly improved following the washout. IPGTT curves were significantly shifted downward in M mice (Fig. 11D), with a corresponding reduction in glucose AUC (Fig. 11E) and significant diet and time×diet interaction effects (Fig. 11F). A similar improvement was observed in F mice (Fig. 11J–L), with reduced AUC after washout (Fig. 11K) and significant diet effects (Fig. 11L), although the interaction term was comparatively weaker. Remarkably, these metabolic changes translated into sex-divergent cognitive outcomes. In M mice, the washout was associated with a robust recovery of recognition memory, as shown by increased discrimination and preference indices in the NOR tasks (Fig. 11M), whereas Y-maze performance and exploratory activity were largely unchanged (Fig. 11N). In contrast, F mice show no cognitive improvement after dietary normalization, with no significant changes in NOR indices (Fig. 11O) and Y-maze measures (Fig. 11P), supporting the concept that HFD-driven cognitive deficits can outlast dietary exposure in F mice.

3.14. Dietary washout is associated with a recovery from HFD-induced molecular alterations in the FC of M mice

Dietary WO did not promote changes of BVRA protein levels (Fig. 12A–B), which remained comparable to those observed in HFD$^{+/+}$8-M. At baseline, a marked increase in activating IRS1 phosphorylation was observed (Fig. 12C). The abnormal activation of the AKT–GSK3β-BAD axis was largely normalized, while the mTOR–P70S6K–S6 axis remained significantly activated (Fig. 12C). This sustained mTOR–P70S6K–S6 axis activity was no longer associated with IRS1 inhibition, suggesting that the function of this branch had shifted from a maladaptive insulin-desensitizing role, toward a revitalized anabolic program. This is supported by the increased PTEN inhibitory phosphorylation (Fig. 12C), that favors PIP_3 accumulation and maintain P70S6K phosphorylation through AKT-independent routes [56–58], thereby sustaining anabolic tone without impairing proximal insulin signaling. Consistently, basal insulin signaling alterations were no longer associated with BVRA levels, suggesting that preservation of BVRA availability permits signaling reorganization and functional

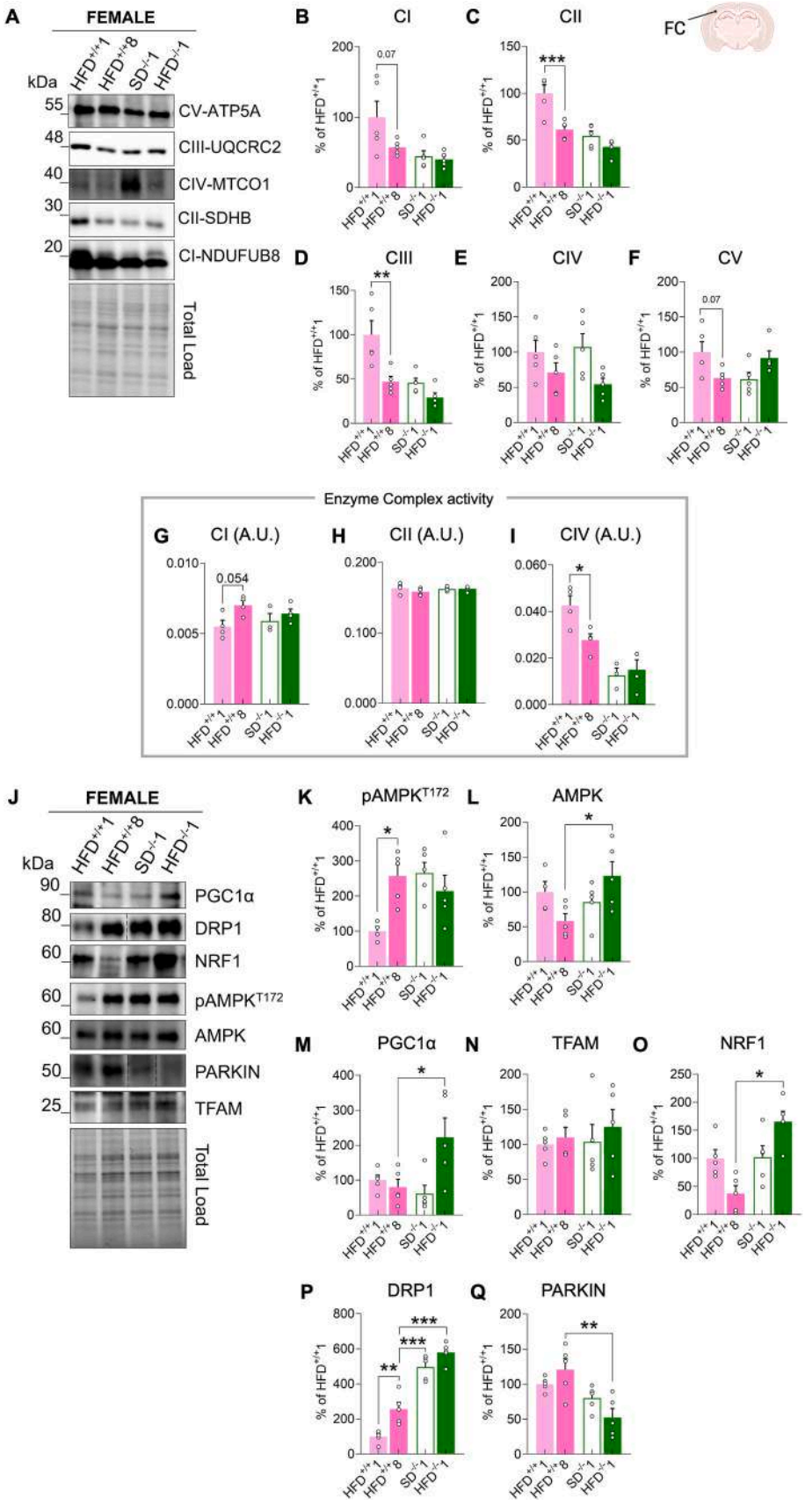

(caption on next page)

Fig. 9. Loss of BVRA leads to mitochondrial impairment in the FC of F mice under metabolic stress
(A-F) Representative Western blot images and densitometric analysis of mitochondrial OXPHOS complexes subunits, i.e., CI (subunit NDUFB8), **C**II (subunit SDHB), **C**III (subunit UQCRC2), **C**IV (subunit MTCO1), **C**V (subunit ATP5A), evaluated in the FC of WT F mice fed with HFD for 1 or 8 weeks and BVRA$^{-/-}$ F mice fed with SD or HFD for 1 week. n = 5 mice/group Values are given as percentage of WT fed with HFD for 1 week set as 100%. Data are presented as means ± SEM. One-way ANOVA with Dunnett's post-hoc test using the HFD$^{+/+}$8 group as reference. *p < 0.05, **p < 0.01, ***p < 0.001.
(G-I) Mitochondrial OXPHOS complexes activity evaluated in the FC of WT F mice fed with HFD for 1 or 8 weeks and BVRA$^{-/-}$ F mice fed with SD or HFD for 1 week. n = 3-4 mice/group. Data are presented as means ± SEM. One-way ANOVA with Dunnett's post-hoc test using the HFD$^{+/+}$8 group as reference. *p < 0.05, **p < 0.01, ***p < 0.001.
(J-Q) Representative Western blot images and densitometric analysis of proteins regulating mitochondrial fitness including, pAMPK^{T172}, total AMPK, PGC1α, TFAM, NRF1, DRP1 and PARKIN levels, evaluated in the FC of WT and BVRA$^{-/-}$ F mice fed with HFD for 1 or 8 weeks and BVRA$^{-/-}$ F mice fed with SD or HFD for 1 week. n = 5 mice/group. Values are given as percentage of WT fed with HFD for 1 week set as 100%. Data are presented as means ± SEM. One-way ANOVA with Dunnett's post-hoc test using the HFD$^{+/+}$8 group as reference. *p < 0.05, **p < 0.01, ***p < 0.001.

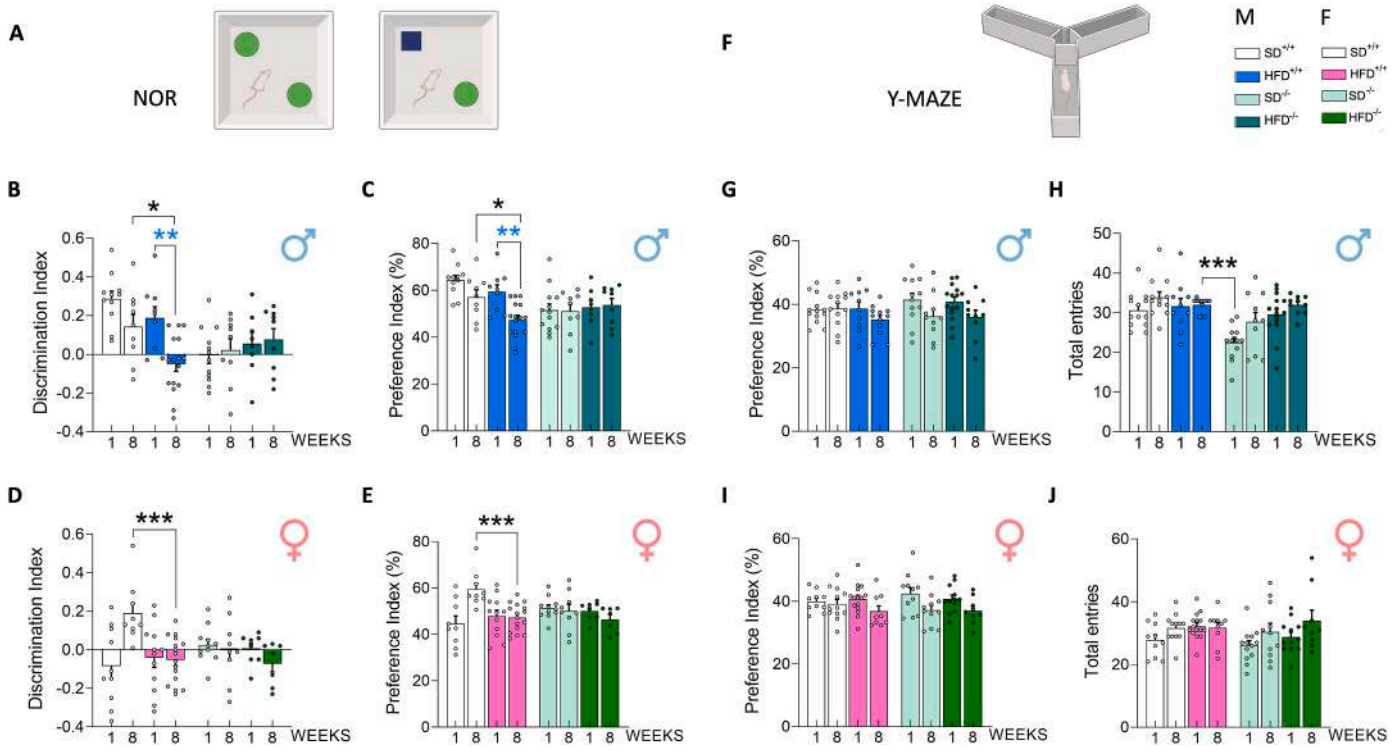

Fig. 10. Outcomes of cognitive tests highlight reduced resilience of F mice.
(A–E) Results of the Novel Object Recognition (NOR) performance performed in WT and BVRA$^{-/-}$ mice (M and F) fed with SD or HFD for either 1 week or 8 weeks. n = 7-16 mice/group. Recognition memory was quantified as Preference Index (PI, % time exploring the novel object) and Discrimination Index (DI), calculated as described in Methods.
(F-J) Results of the Y-maze assessment of short-term spatial working memory and exploratory activity performed in the same experimental groups as in A-D. n = 7-16 mice/group. Working memory was expressed Preference Index (PI, % of time spent exploring the new arm), while locomotor/exploratory drive was estimated by total arm entries.
Data are shown as mean ± SEM. One-way ANOVA with Dunnett's post-hoc test using the HFD$^{+/+}$8 group as reference. *p < 0.05, **p < 0.01, ***p < 0.001.

recovery (Fig. 12D). Acute INI stimulation failed to further enhance signaling activation (Fig. 12E–J), likely due to the robust increase of basal panIRS^{Y} (Fig. 12C), indicating that the pathway had reached a state of maximal upstream engagement. At the mitochondrial level, OXPHOS subunit levels were restored (Fig. 12K–L) and complex activities were preserved (Fig. 12M). AMPK phosphorylation and protein levels remained stable, while a reduction in biogenesis markers was observed (Fig. 12M-O). DRP1 levels, elevated in HFD+/+8-M mice, were significantly reduced after washout (Fig. 12M-O), while PARKIN levels were strongly increased (Fig. 12M-O), supporting the hypothesis about a resolution of the fission-driven program and enhanced mitophagy engagement, along with an improved mitochondrial quality control. Together, these findings indicate that preservation of BVRA levels after dietary normalization enables coordinated recovery of cortical insulin signaling, mitochondrial homeostasis, and cognitive function in M mice.

3.15. Metabolic stress-induced alterations outlast dietary exposure in the FC of F mice

In WT F mice, dietary normalization (WO) further reduced BVRA levels in the FC (Fig. 13A–B). Under basal conditions, WO mice displayed increased IRS1 activating phosphorylation and reduced IRS1 inhibition, suggesting an apparent recovery of upstream insulin sensitivity. However, this change was not reflected in downstream components. The AKT–GSK3β axis remained abnormally elevated (Fig. 13C), and a further increase in mTOR-P70S6K-S6 axis activation was observed (Fig. 13C). PTEN inhibitory phosphorylation was markedly elevated, to a greater extent than in M mice (Fig. 13C). Together, these alterations reflect a maladaptive activation, in sharp contrast to the basal signaling recovery observed in M mice. Reduced BVRA protein levels following the washout were significantly associated with basal insulin signaling alterations (Fig. 13D). Upon acute INI stimulation, the signaling defects

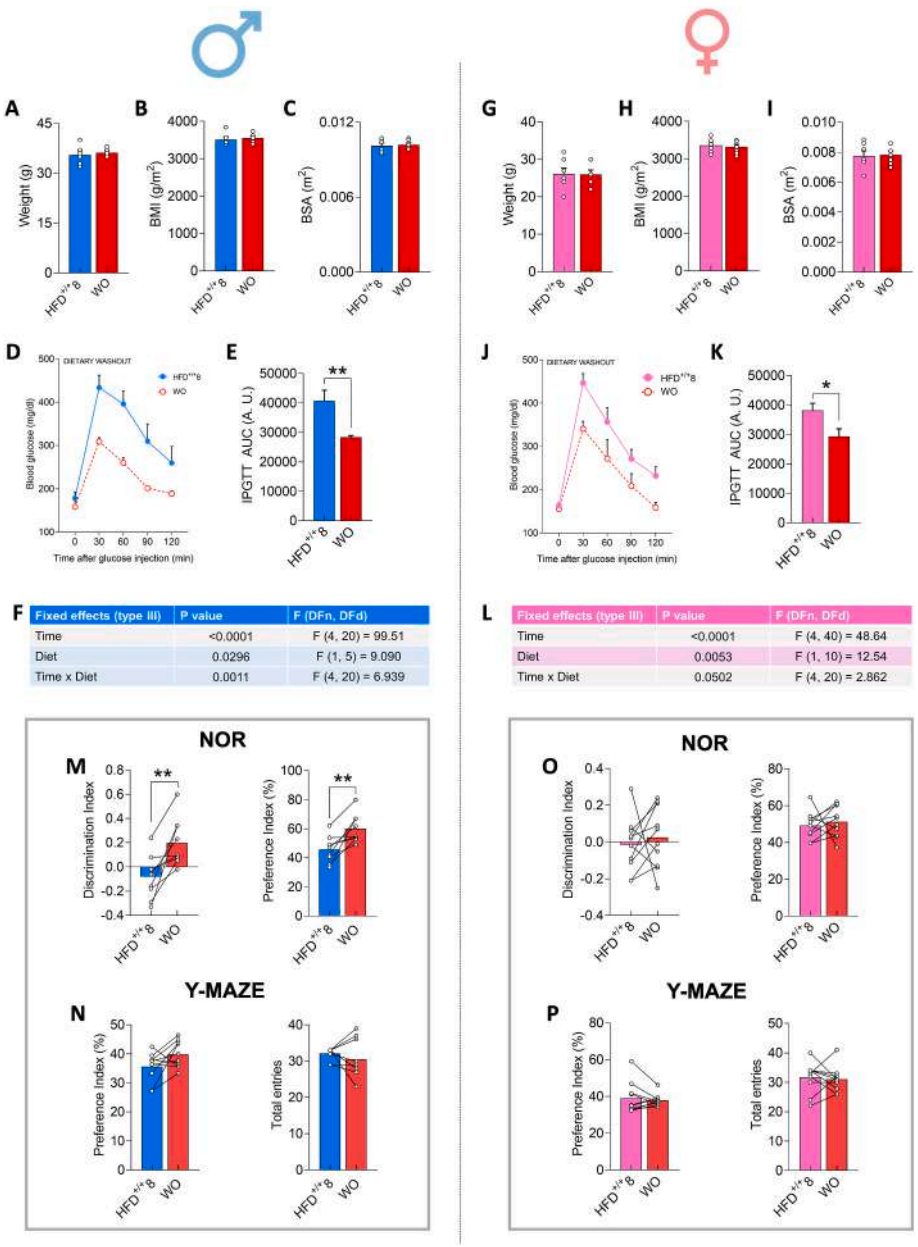

Fig. 11. Diet wash-out effects on peripheral metabolic parameters and cognitive tests.
(A-C) Body weight (g), body mass index (BMI, g/m^2), body surface area (BSA, m^2), evaluated in WT M mice fed with HFD for 8 weeks and further challenged with a standard diet for additional 8 weeks (WO). n = 6 mice/group. Student t-test.
(D) Intraperitoneal glucose tolerance test (IPGTT) evaluated in WT M mice fed with HFD for 8 weeks and further challenged with a standard diet for additional 8 weeks (WO). n = 6 mice/group.
(E) Area Under Curve (AUC) relative to the IPGTT performed in WT M mice fed with HFD for 8 weeks and further challenged with a standard diet for additional 8 weeks (WO). n = 6 mice/group. Student t-test. **p < 0.01.
(F) Results of the Three-way ANOVA relative to the IPGTT performed in WT M mice.
(G-I) Body weight (g), body mass index (BMI, g/m^2), body surface area (BSA, m^2), evaluated in WT F mice fed with HFD for 8 weeks and further challenged with a standard diet for additional 8 weeks (WO). n = 7 mice/group. Student t-test.
(J) Intraperitoneal glucose tolerance test (IPGTT) evaluated in WT F mice fed with HFD for 8 weeks and further challenged with a standard diet for additional 8 weeks (WO). n = 7-11 mice/group.
(K) Area Under Curve (AUC) relative to the IPGTT performed in WT F mice fed with HFD for 8 weeks and further challenged with a standard diet for additional 8 weeks (WO). n = 7-11 mice/group. Student t-test. *p < 0.05.
(L) Results of the Three-way ANOVA relative to the IPGTT performed in WT F mice.
(M – N) Novel Object Recognition (NOR) and) Y-maze tests performed in WT M mice fed with HFD for 8 weeks and further challenged with a standard diet for additional 8 weeks (WO). n = 10 mice/group. Student t-test. **p < 0.01
(O-P) Results of the Novel Object Recognition (NOR) and Y-maze tests performed in WT F mice fed with HFD for 8 weeks and further challenged with a standard diet for additional 8 weeks (WO). n = 10 mice/group. Student t-test. **p < 0.01.

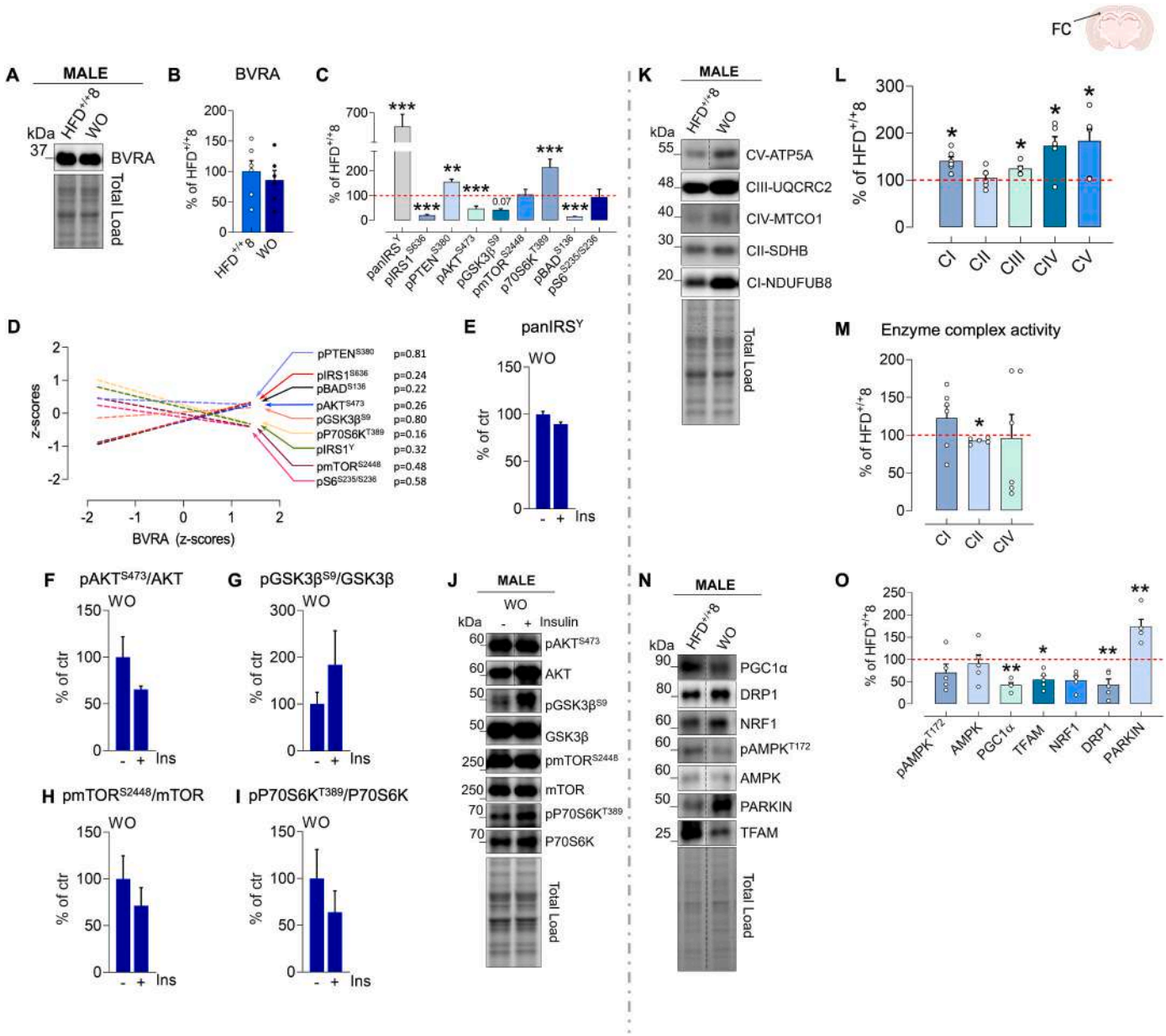

Fig. 12. Dietary washout is associated with a recovery from HFD-induced molecular alterations in the FC of M mice.

WT M mice were fed with HFD for 8 weeks and further challenged with a standard diet for additional 8 weeks (WO), and the following parameters were evaluated:

(A-B) Representative Western blot images and densitometric evaluation of BVRA protein levels. n = 5 mice/group. Values are given as percentage of $HFD^{+/+}$8-M set as 100%. Mean ± SEM.

(C) Levels of proteins of the insulin signaling. n = 6 mice/group. Values are given as percentage of $HFD^{+/+}$8-M set as 100%. Mean ± SEM. Student *t*-test: *p < 0.05, **p < 0.01, **p < 0.001.

(D) Pearson correlations between BVRA protein levels and proteins of the insulin signaling evaluated in the FC of WT M mice. Significant correlations are reported in red. p values are shown.

(E-J) Densitometric evaluation and representative Western blot images relative to the activation of proteins of the insulin signaling pathway evaluated in the FC of WT M mice following INI administration at the end of the washout (WO) period. AKT activation was evaluated as $pAKT^{S473}$/AKT ratio; GSK3β inhibition was evaluated as $pGSK3\beta^{S9}$/GSK3β ratio; mTOR activation was evaluated as $pmTOR^{S2448}$/mTOR ratio; and P70S6K activation was evaluated as $pP70S6K^{T389}$/P70S6K ratio. n = 4 mice/group. Values are given as percentage of vehicle set as 100%. Data presented as mean ± SEM. Student *t*-test: *p < 0.05, **p < 0.01, **p < 0.001. (−) vehicle; (+): insulin 1IU.

(K-L) Representative Western blot images and densitometric analysis of mitochondrial OXPHOS complexes subunits, i.e., CI (subunit NDUFB8), **C**II (subunit SDHB), **C**III (subunit UQCRC2), **C**IV (subunit MTCO1), **C**V (subunit ATP5A). n = 6 mice/group. Values are given as percentage of $HFD^{+/+}$8-M set as 100%. Mean ± SEM. Student *t*-test: *p < 0.05.

(M) Mitochondrial OXPHOS complexes activity evaluated in the FC of WT M mice. n = 6 mice/group. Values are given as percentage of $HFD^{+/+}$8-M set as 100%. Mean ± SEM. Student *t*-test: *p < 0.05.

(N-O) Representative Western blot images and densitometric analysis of proteins regulating mitochondrial fitness including, $pAMPK^{T172}$, total AMPK, PGC1α, TFAM, NRF1, DRP1 and PARKIN levels, evaluated in the FC of WT M mice. n = 5 mice/group. Values are given as percentage of $HFD^{+/+}$8-M set as 100%. Mean ± SEM. Student *t*-test: *p < 0.05, **p < 0.01.

became even more pronounced: panIRS1^{Y} levels increased further, yet no activation of AKT or its downstream effectors was detected (Fig. 13E–J), indicating a complete functional disconnection between proximal and distal nodes of the pathway. This pattern defines an aggravated state of post-receptor insulin resistance. In contrast to M mice, where the lack of INI responsiveness can be explained by the maximal basal IRS1 engagement and basal signaling recovery, the failure of AKT activation in F mice despite increased IRS1 activation following INI, reflects a state of insulin resistance consequent to the absence of basal signaling rescue. At the mitochondrial level, the consequences were equally detrimental. OXPHOS subunits, particularly CV, remained reduced (Fig. 13K–L), and the activities of CII and CIV declined further compared to HFD$^{+/+}$8-F (Fig. 13M), revealing a progressive OXPHOS deterioration. AMPK phosphorylation was strongly reduced, while AMPK levels increase (Fig. 13N–O), indicating the absence of compensatory non-transcriptional mechanisms. NRF1 and TFAM levels were elevated (Fig. 13N–O), suggesting that the transcriptional biogenesis response was maintained despite reduced AMPK activation. DRP1 levels remained elevated after washout (Fig. 13N–O) while PARKIN levels decreased significantly (Fig. 13N–O), supporting the hypothesis that sustained mitochondrial fission might occur without mitophagy clearance, finally resulting in the accumulation of dysfunctional mitochondria. Hence, in F mice, HFD-induced alterations outlast dietary exposure in the FC, with further BVRA reduction driving persistent insulin-signaling uncoupling and progressive mitochondrial deterioration — a trajectory absent in M mice and that highlight how metabolic stress can even seed long-lasting functional consequences.

3.16. Metabolic stress-induced alterations outlast dietary exposure in the HIP in a sex-dependent manner

Dietary normalization revealed a marked sex-dependent persistence of HIP metabolic alterations. In M mice dietary WO was associated with a further reduction of BVRA levels in the HIP (Supplementary Fig. 17A–B). Although basal upstream insulin signaling appeared partially recovered, as indicated by increased panIRS1^{Y} levels (Supplementary Fig. 17C) and reduced pIRS1^{S636} levels (Supplementary Fig. 17C), downstream signaling remained persistently uncoupled. The AKT–mTOR–P70S6K axis remained hyper-activated (Supplementary Fig. 17C) and failed to respond appropriately to acute INI stimulation (Supplementary Fig. 17E–J), supporting a state of insulin resistance. At the mitochondrial level, the dietary washout exacerbated the dysfunctions, with reduced CIV abundance (Supplementary Fig. 17K–L) and decreased activities of CII and CIV (Supplementary Fig. 17M), despite activation of a transcriptional biogenetic response marked by increased NRF1 and TFAM levels (Supplementary Fig. 17N–O). This profile closely resembled that observed in SD$^{-/-}$1-M, supporting the concept that progressive BVRA loss shifts the HIP from an adaptive to a maladaptive metabolic state.

In F mice, HIP vulnerability emerged even more strikingly after dietary normalization. While HFD did not induce overt HIP basal alterations at the end of the dietary period, washout resulted in a pronounced reduction of BVRA levels (Supplementary Fig. 18A–B) and unveiled persistent defects in both basal (Supplementary Fig. 18C) and acute insulin signaling (Supplementary Fig. 18E–J). These alterations were characterized by upstream IRS1 engagement uncoupled from downstream AKT-dependent signaling, together with aberrant activation of GSK3β and mTOR. Mitochondrial dysfunction was severe, with widespread OXPHOS subunits levels reduction (Supplementary Fig. 18K–L), impaired complexes activities (Supplementary Fig. 18M), and activation of a transcriptional biogenesis program (Supplementary Fig. 18N–O) that failed to restore mitochondrial efficiency. These alterations emerged exclusively after the washout, indicating that short-term metabolic stress imprints a delayed and long-lasting molecular instability in the F HIP that becomes manifest only after removal of the stressor.

Together, these findings identify the HIP as a delayed but highly vulnerable target of metabolic stress once BVRA-dependent compensatory capacity is exceeded, with F mice exhibiting a pronounced susceptibility to post-dietary metabolic deterioration.

3.17. Hepatic molecular remodeling persists after dietary washout

In M mice, the WO promoted a global attenuation of insulin signaling, with reduced phosphorylation of IRS1, AKT, and downstream effectors (Supplementary Fig. 19A–D), consistent with a resetting of hepatic signaling tone toward a lower baseline activity. At the mitochondrial level, dietary washout was also associated with a remodeling of mitochondrial components. OXPHOS subunit expression levels remained largely preserved, with the notable exception of a further increase in CIV abundance (Supplementary Fig. 19F). In parallel, respiratory complex activity showed a remodeled profile, characterized by reduced CI and CII activities together with increased CIV activity compared with HFD+/+8 mice (Supplementary Fig. 19G). This pattern was accompanied by the activation of transcriptional biogenesis markers, including PGC1α and TFAM, together with reduced DRP1 levels, without a corresponding normalization of respiratory complex activity (Supplementary Fig. 19H–I). These findings are coherent with the hypothesis that, even in a metabolically resilient organ such as the LIV, short-term metabolic stress is sufficient to induce mitochondrial changes that persist beyond dietary exposure.

In F mice, dietary washout was associated with a persistent hepatic molecular remodeling. BVRA protein levels declined further after dietary normalization (Supplementary Fig. 20A–B), and insulin signaling exhibited a peculiar profile characterized by reduced IRS1 inhibition and increased PTEN inhibitory phosphorylation uncoupled from effective downstream targets activation (Supplementary Fig. 20C). Remarkably, reduced BVRA levels were significantly associated with these signaling alterations (Supplementary Fig. 20D). Notably, this further reduction of hepatic BVRA occurred in parallel with improved systemic glucose tolerance after dietary washout. This pattern is consistent with the improved glucose handling observed in BVRA$^{-/-}$ F mice under HFD and supports the possibility that, in females, a marked reduction of hepatic BVRA levels may participate in an adaptive metabolic response. However, these data alone do not allow us to explain improved systemic glucose tolerance solely on the basis of BVRA reduction, thus supporting a cautious interpretation of LIV-specific BVRA function. Mitochondrial proteins showed persistent changes consistent with an adaptive response (Supplementary Fig. 20E–G), along with reduced levels of biogenetic regulators, and a shift toward increased mitochondrial fragmentation without adequate mitophagy (Supplementary Fig. 20H–I).

Overall, hepatic insulin signaling and mitochondrial-related changes followed distinct trajectories after dietary normalization, suggesting that BVRA availability may influence the processes associated with long-term hepatic adaptation.

4. Discussion

The findings reported here support a model in which BVRA deficiency is associated with brain region- and sex-dependent metabolic vulnerability that emerges before canonical markers of insulin resistance and mitochondrial failure become fully apparent. By combining a short-term dietary stress with genetic BVRA deletion, we identify a vulnerability trajectory across FC and HIP that parallels differences in BVRA abundance and follows a molecular sequence that differs among brain regions and sexes. This temporal ordering suggests that BVRA is not merely a passive readout of metabolic impairment but may contribute to the molecular threshold that influences when, where, and how metabolic stress translates into cellular dysfunction. Consistent with emerging evidence that brain insulin action is regionally heterogeneous [59], the FC emerges as the earliest and most vulnerable region, displaying insulin resistance and mitochondrial remodeling after HFD

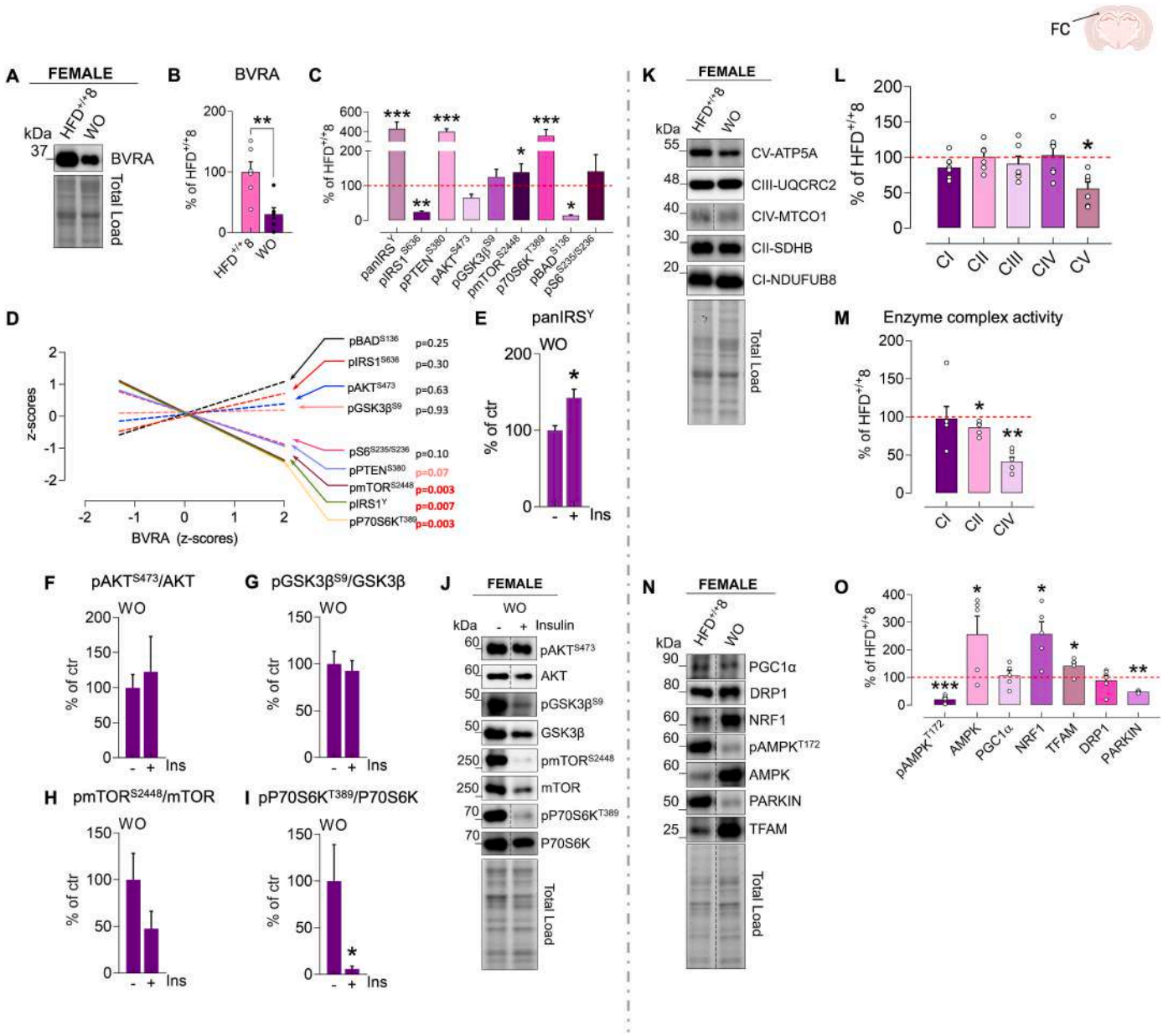

Fig. 13. Dietary washout is not associated with a recovery from HFD-induced molecular alterations in the FC of F mice.

WT F mice were fed with HFD for 8 weeks and further challenged with a standard diet for additional 8 weeks (WO), and the following parameters were evaluated:

(A-B) Representative Western blot images and densitometric evaluation of BVRA protein levels. n = 5 mice/group. Values are given as percentage of $HFD^{+/+}8$-F set as 100%. Mean ± SEM.

(C) Levels of proteins of the insulin signaling. n = 6 mice/group. Values are given as percentage of $HFD^{+/+}8$-F set as 100%. Mean ± SEM. Student *t*-test: *p < 0.05, **p < 0.01, **p < 0.001.

(D) Pearson correlations between BVRA protein levels and proteins of the insulin signaling evaluated in the FC of WT F mice. Significant correlations are reported in red. p values are shown.

(E-J) Densitometric evaluation and representative Western blot images relative to the activation of proteins of the insulin signaling pathway evaluated in the FC of WT F mice following INI administration at the end of the washout (WO) period. AKT activation was evaluated as $pAKT^{S473}$/AKT ratio; GSK3β inhibition was evaluated as $pGSK3\beta^{S9}$/GSK3β ratio; mTOR activation was evaluated as $pmTOR^{S2448}$/mTOR ratio; and P70S6K activation was evaluated as $pP70S6K^{T389}$/P70S6K ratio. n = 4 mice/group. Values are given as percentage of vehicle set as 100%. Data presented as mean ± SEM. Student *t*-test: *p < 0.05, **p < 0.01, **p < 0.001. (−) vehicle; (+): insulin 1IU.

(K-L) Representative Western blot images and densitometric analysis of mitochondrial OXPHOS complexes subunits, i.e., CI (subunit NDUFB8), **C**II (subunit SDHB), **C**III (subunit UQCRC2), **C**IV (subunit MTCO1), **C**V (subunit ATP5A). n = 6 mice/group. Values are given as percentage of $HFD^{+/+}8$-F set as 100%. Mean ± SEM. Student *t*-test: *p < 0.05.

(M) Mitochondrial OXPHOS complexes activity evaluated in the FC of WT F mice. n = 6 mice/group. Values are given as percentage of $HFD^{+/+}8$-M set as 100%. Mean ± SEM. Student *t*-test: *p < 0.05.

(N-O) Representative Western blot images and densitometric analysis of proteins regulating mitochondrial fitness including, $pAMPK^{T172}$, total AMPK, PGC1α, TFAM, NRF1, DRP1 and PARKIN levels, evaluated in the FC of WT F mice. n = 5 mice/group. Values are given as percentage of $HFD^{+/+}8$-M set as 100%. Mean ± SEM. Student *t*-test: *p < 0.05, **p < 0.01.

exposure. The HIP, which shows higher basal BVRA abundance, displays delayed and attenuated alterations, consistent with a relatively greater metabolic resilience in this experimental context. Yet this resilience is conditional: BVRA deficiency accelerates HIP vulnerability to a degree that would otherwise require prolonged dietary exposure. Interestingly, the LIV, that we used as peripheral tissue comparator, was characterized by high basal BVRA levels, and displayed a more complex phenotype: insulin signaling alterations were modest and non-canonical, whereas selected respiratory complex activities and mitochondrial-related markers were altered. This pattern is better interpreted as hepatic adaptive remodeling rather than overt hepatic insulin resistance [54,55,60–62].

A key mechanistic insight is that BVRA downregulation constitutes an early molecular signature of impaired insulin responsiveness, detectable before canonical markers such as inhibitory IRS1 phosphorylation become apparent. This concept is consistent with evidence that BVRA is not a merely heme catalytic enzyme but a multifunctional regulator at the interface of insulin signaling, redox control, and mitochondrial homeostasis [12]. Our study further extends current knowledge by showing that the brain can develop insulin resistance as BVRA levels decline even in the absence of overt canonical IRS1 inhibition. INI administration was critical to unmasking this latent resistance in regions where canonical insulin resistance markers were not increased at the basal level, including the female FC and the male HIP after short-term HFD [34,39,44]. Furthermore, in the female HIP, the acute INI stimulation promotes a reduction of BVRA levels and uncovers latent insulin resistance, despite preserved basal BVRA levels, supporting the hypothesis that BVRA availability might contribute to the threshold for signaling competence. These results confirm, and extend to the brain, previous findings collected in obese subjects showing that BVRA levels change dynamically in response to insulin, and greater BVRA variations occur in those subjects with lower insulin sensitivity [25,29]. This event represents a double-edge sword because while BVRA reduction favors IRS1 activation, it impairs downstream signal activation, and thus reduces insulin-mediated effects [12]. We also report for the first time that loss of BVRA is associated with increased PTEN activation (reduced $pPTEN^{S380}$). Mechanistically, PTEN is a key upstream brake on the AKT–mTOR signaling, thereby setting the basal inhibitory tone of insulin signaling propagation [63]. Beyond metabolism, in the brain PTEN governs neuronal growth, synaptic homeostasis and stress responses [63]. This BVRA-PTEN association could amplify region- and sex-specific vulnerability under metabolic challenge. Hence, under metabolic stress, BVRA is dynamically regulated in a way that likely aims to favor IRS1 sensitization upstream in the signaling, yet ultimately limits the coordinated activation of downstream effectors, resulting in insulin resistance. These findings support the interpretation that BVRA loss is an early event associated with subsequent insulin unresponsiveness before canonical markers become detectable.

Remarkably, we also found that insulin signaling defects precede oxidative distress across FC, HIP and LIV, a dissociation that challenges the view of mitochondrial dysfunction and redox imbalance as primary drivers of brain insulin resistance [64–66]. Rather, our results are consistent with the possibility that mitochondrial dysfunction and redox imbalance emerge downstream of, or in parallel with, altered BVRA-associated signaling. Furthermore, because BVRA catalyzes the conversion of biliverdin into bilirubin, the redox phenotype observed in $BVRA^{-/-}$ mice may reflect reduced bilirubin-dependent antioxidant buffering. This interpretation is consistent with previous evidence showing that endogenous bilirubin acts as a physiologically relevant antioxidant, particularly against superoxide, and that loss of BVRA-dependent bilirubin production increases susceptibility to oxidative stress [19,23]. Accordingly, the increase in 4-HNE, 3-NT, and protein carbonyls observed mainly in $BVRA^{-/-}$ mice likely reflects the combined impact of chronic BVRA loss on bilirubin-dependent redox protection and BVRA-associated signaling/mitochondrial pathways. In WT mice, relatively small BVRA variations were associated with altered insulin signaling activation, whereas overt mitochondrial impairment requires a broader loss of BVRA. This threshold is also sex-biased, as F mice display a greater mitochondrial vulnerability than M mice, most evident in the FC, even in the presence of comparatively milder insulin signaling alterations. Consistently, a previous work showed a greater reduced expression of mitochondrial unfolded protein response (UPRmt) genes in female hypothalamus with respect to male in response to HFD [48].

The sex-dependent pattern of metabolic vulnerability represents a central finding of our study. Female mice developed cognitive impairments comparable to those observed in M mice despite milder or delayed molecular alterations — a dissociation between molecular trajectory and functional outcome that persisted across brain regions and dietary conditions. This female cognitive vulnerability in the context of milder basal insulin resistance points to a differential sensitivity of neural circuits to BVRA-dependent signaling disruption that warrants further investigation, and is consistent with the well-documented female predominance in AD risk and progression [67–70]. Beyond its role in brain insulin signaling, BVRA also exerts a direct synaptic function in the HIP, acting as a molecular scaffold that bridges focal adhesion kinase to Src to support NMDA-receptor–mediated synaptic plasticity; its loss impairs long-term potentiation and cognitive performance [44,71]. This provides an additional, insulin-independent route through which BVRA deficiency may compromise cognition. Notably, recognition memory improved in M mice after dietary normalization despite the persistence of hippocampal alterations. This apparent dissociation may reflect the distributed circuitry underlying the novel object recognition task, which primarily relies on perirhinal cortical processing but can additionally engage hippocampal and prefrontal networks depending on task demands and retention interval. Because the present paradigm assessed long-term recognition memory, the contribution of prefrontal circuits may be particularly relevant, potentially explaining why behavioral recovery can occur despite persistent hippocampal molecular alterations [72,73].

A further consideration concerns the cellular origin of the insulin signaling alterations detected in brain tissue. Because our analyses were performed on whole-tissue lysates, the measured changes in insulin signaling and downstream reflect the aggregate contribution of all resident cell populations and cannot be attributed to a specific compartment. This distinction is increasingly relevant, as glial insulin signaling has emerged as a critical modulator of brain metabolic and inflammatory homeostasis [47,74]. In particular, loss of insulin signaling in microglia has been shown to impair Aβ clearance and to exacerbate neuroinflammation and AD-like neuropathology, while dysregulated insulin signaling in neurons and astrocytes has likewise been implicated in cognition and AD pathogenesis [47,74]. Accordingly, the BVRA-dependent insulin-signaling changes described here likely reflect the combined and potentially divergent responses of neuronal and glial populations, a dimension that will require cell-type-resolved approaches to be fully dissected.

AMPK-driven mitochondrial adaptation was identified as a conceivable mechanistic pattern for the sex bias we observed. AMPK is a central energetic stress integrator that preserves mitochondrial fitness by coordinating acute quality-control responses (e.g., mitochondrial dynamics and autophagy/mitophagy) and, under sustained challenge, a transcriptional rebuilding program (biogenesis via PGC1α/NRF1/TFAM) [50,51,75]. In addition, AMPK control is temporally layered, coupling rapid post-translational quality control to slower rebuilding outputs [51]. The male brain appears more resilient toward mitochondrial alterations, as BVRA loss both in $HFD^{+/+}8$ and in $BVRA^{-/-}$, regardless of diet, engages AMPK-associated compensatory programs that help maintaining OXPHOS efficiency despite the development of insulin resistance. By contrast, F mice show a sharper mitochondrial liability: loss of BVRA is associated with bioenergetic dysfunction despite AMPK engagement, both in WT and $BVRA^{-/-}$ mice suggesting that mitochondrial adaptation mechanisms are either less effectively

recruited or more rapidly exhausted. Activation of the fission process in M mice (elevated DRP1 without parallel PARKIN induction) seems to further support OXPHOS, whereas the same response is associated with progressive CIV failure in F mice, highlighting a sex-specific inability to mount an effective mitochondrial adaptation. Sex-dependent differences in brain mitochondrial function and redox homeostasis have been reported in multiple contexts [76,77], and our data extend this to a BVRA-regulated axis in which the female brain is intrinsically more susceptible to mitochondrial failure under metabolic challenges.

Dietary normalization revealed that the molecular consequences of short-term HFD are not fully reversible, uncovering a form of BVRA-dependent metabolic memory. Male mice showed a rescue in the FC accompanied by cognitive improvement, while the HIP remained largely refractory. The female response was more severe and widespread. A progressive insulin signaling uncoupling, and deteriorating mitochondrial function, with no cognitive recovery, that outlast HFD consumption, were observed. This region- and sex-specific persistence of metabolic alterations tracked with continued BVRA decline, suggesting that BVRA loss itself encodes metabolic memory by sustaining signaling uncoupling and impairing mitochondrial quality control beyond the period of dietary insult. Importantly, convergent human evidence supports the plausibility of this concept. In healthy-weight men, just five days of calorie-rich overfeeding was sufficient to impair brain insulin action, and reduced insulin responsiveness in cognitive-related regions (particularly in the HIP) remained detectable one week after returning to a regular diet, in the absence of overt changes in body weight or peripheral insulin sensitivity [78]. Furthermore, very recent population-level evidence indicates that adherence to healthier dietary patterns leads to a gain in life expectancy in both sexes, yet the estimated benefit is smaller in women, consistent with a sex-dependent responsiveness to diet quality [79]. These data reinforce our hypothesis that even short-term metabolic insults can leave a persistent, brain region-selective signature that outlasts the diet exposure period, and that the failure to restore the putative BVRA-dependent buffering capacity may contribute a key factor sustaining vulnerability.

The above-mentioned differences were not fully explained by divergent systemic metabolic profiles in our study, as both sexes exhibited comparable body weight and fasting glycemia under short-term HFD. A striking observation was the fact that $HFD^{-/-}$ F mice were protected from HFD-induced glucose intolerance, whereas $HFD^{-/-}$ M mice did not show any worsening with respect to $HFD^{+/+}$ mice, suggesting that BVRA deficiency does not impair systemic glucose handling, at least in a short time window. These findings likely support a dissociation between whole-body glucose handling and tissue-specific molecular responses. Although $HFD^{-/-}$ F mice showed improved glucose tolerance under HFD, this systemic phenotype was not paralleled by preserved molecular homeostasis in brain regions, where altered insulin signaling competence and mitochondrial adaptation were observed. Therefore, systemic glucose tolerance should not be interpreted as a direct proxy of brain metabolic resilience.

Rather, the LIV's greater resilience to HFD-induced insulin signaling alterations might be consistent with its higher basal BVRA abundance relative to the brain, potentially providing a larger redox–metabolic buffering reserve [80]. However, the hepatic phenotype should be interpreted cautiously and is more consistent with adaptive remodeling than with overt hepatic insulin resistance. Under short-term HFD, the LIV showed selected changes in respiratory complex activities and mitochondrial-related proteins, but these changes occurred in the absence of a canonical insulin resistance signature and were not associated with impaired systemic glucose handling [55]. This interpretation agrees with previous evidence linking hepatic BVRA loss to altered lipid metabolism and steatotic phenotypes in more severe or prolonged metabolic contexts [21,23,24,38], and with the current view that metabolic dysfunction-associated steatotic liver disease (MASLD) reflects an integrated systemic-hepatic process involving altered hepatic insulin signaling, hyperinsulinemia, hepatic insulin clearance, adipose-derived substrate flux, de novo lipogenesis, and mitochondrial bioenergetic adaptation [81,82]. Hence, the present short-term paradigm does not allow us to conclude whether BVRA exerts a beneficial or detrimental role in hepatic glucose handling.

The washout data reinforce this interpretation. In $HFD^{+/+}$ F mice, hepatic BVRA declined further after dietary normalization, whereas systemic glucose tolerance improved. Thus, although this pattern is consistent with the possibility that reduced hepatic BVRA participates in an adaptive metabolic response in female mice, the systemic glycemic curve cannot be used alone to infer the role of hepatic BVRA in either direction. In this context, the milder and non-canonical hepatic phenotype compared with brain regions is compatible with greater hepatic metabolic adaptation. Dietary washout further revealed sex-associated differences in hepatic insulin signaling and mitochondrial-related readouts. In M mice, dietary normalization was associated with a normalization of hepatic insulin signaling along with alterations of mitochondrial activities, whereas in F mice both insulin signaling and OXPHOS activities remained altered. These findings support the interpretation that the hepatic phenotype reflects an adaptive remodeling phase, in which mitochondrial remodeling represents a slower step in metabolic normalization [83,84].

5. Conclusions

This study defines BVRA as a sex- and brain region-specific determinant of vulnerability to HFD feeding, with the most consistent effects observed in the brain (Fig. 14). In the brain, insulin resistance emerges early and is mechanistically associated with BVRA depletion before canonical markers of metabolic disease appear, with M mice showing more pronounced basal molecular alterations and F mice displaying a dissociation between milder molecular changes and equivalent cognitive impairment. The FC represents the earliest and most vulnerable brain region, whereas the HIP shows delayed and more context-dependent alterations, supporting a brain regional vulnerability to HFD feeding. Peripheral hepatic analyses revealed a distinct adaptive profile following loss of BVRA, in which selected insulin-signaling and mitochondrial-related readouts were altered without clear evidence of overt hepatic insulin resistance or impaired systemic glucose handling. Thus, the LIV findings are best interpreted as a peripheral adaptive remodeling response within the present short-term HFD paradigm. Dietary normalization further revealed sex-dependent differences in recovery trajectories. In M mice, cortical insulin-signaling and mitochondrial-related readouts partially recovered in parallel with improved recognition memory, whereas in F mice BVRA levels continued to decline and molecular alterations persisted together with cognitive impairment. These findings support the concept that short-term HFD feeding can imprint a BVRA-associated molecular memory in brain regions, particularly in F mice. Overall, targeting the BVRA-regulated axis may represent a strategy to restore brain metabolic and cognitive resilience in the context of high-fat diet feeding, aging, and neurodegenerative disease.

6. Limitations of the study

Several limitations should be acknowledged. First, the use of constitutive BVRA knockout mice prevents attribution of the observed phenotypes exclusively to brain-intrinsic BVRA loss, and region-selective rescue experiments will be required to establish causal sufficiency. Therefore, the differences observed between FC and HIP should be interpreted as region-associated molecular phenotypes emerging in the context of whole-body BVRA deficiency and HFD exposure, rather than as definitive evidence of BVRA action within specific brain regions. Future studies using brain-specific BVRA rescue, will be required to define the direct contribution of local BVRA signaling to these phenotypes. Second, the hormonal basis of the sex dimorphism remains unexplored; estrogen is known to regulate both mitochondrial

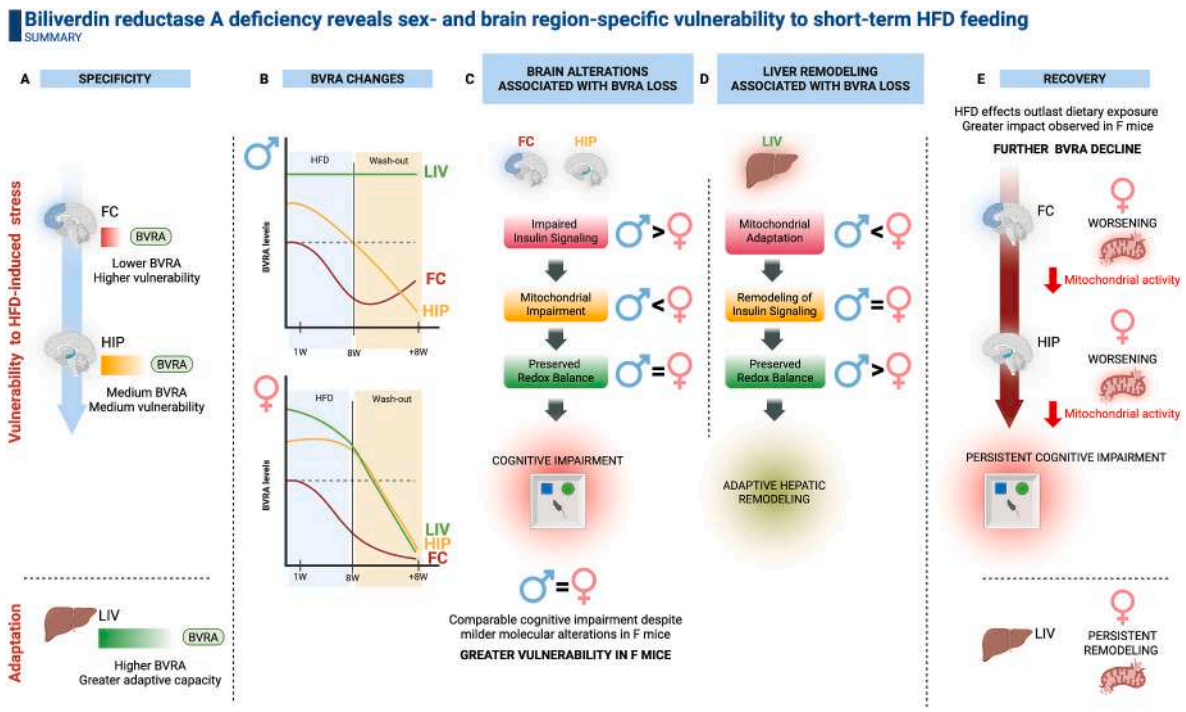

Fig. 14. BVRA deficiency is associated with sex- and brain region-dependent vulnerability to short-term high-fat diet feeding.
Schematic summary of the proposed model linking BVRA abundance to sex- and brain region-specific vulnerability during high-fat diet (HFD) exposure and dietary normalization, with the liver included as a peripheral metabolic comparator.
(A) Basal BVRA abundance parallels a brain region-specific gradient of vulnerability to HFD-induced stress. The frontal cortex (FC), characterized by lower BVRA levels, represents the most vulnerable region, whereas the hippocampus (HIP) displays intermediate vulnerability. The liver (LIV), which shows higher BVRA abundance, exhibits greater adaptive capacity and metabolic buffering.
(B) HFD-induced BVRA decline is associated with sex- and brain region-specific vulnerability. BVRA reduction emerges prominently in the FC, is delayed or less pronounced in the HIP, and shows a distinct trajectory in the LIV, with divergent male and female responses during the washout phase.
(C) BVRA loss is associated with brain region-specific molecular alterations. In brain regions, impaired insulin signaling represents the most severely affected pathway, followed by an intermediate degree of mitochondrial alterations, whereas redox balance is largely preserved, ultimately contributing to cognitive impairment. Symbols indicate whether alterations were more pronounced in M mice or in F mice: although M mice display more pronounced molecular alterations in several pathways, F mice develop comparable cognitive deficits, indicating greater functional vulnerability.
(D) In the liver, BVRA loss is associated with mitochondrial adaptation, remodeling of insulin signaling, and preserved redox balance. These hepatic changes are interpreted as adaptive hepatic remodeling rather than as evidence of hepatic vulnerability, mitochondrial impairment, or overt hepatic insulin resistance.
(E) Dietary normalization fails to fully reverse HFD-induced alterations in F mice. In F mice, HFD effects outlast dietary exposure and are associated with further BVRA decline, persistent molecular alterations in the FC and HIP, reduced mitochondrial activity, and persistent cognitive impairment. In the LIV, dietary normalization is associated with further reduction of BVRA protein levels and persistent mitochondrial remodeling in F mice.
Overall, the model supports the hypothesis that BVRA may contribute to a molecular buffering system influencing the timing, severity, and reversibility of HFD-induced brain responses in a sex- and region-specific manner, while hepatic changes are best interpreted as adaptive remodeling within the present short-term HFD paradigm.

bioenergetics and insulin sensitivity [85,86], and ovariectomy or hormone replacement paradigms will be necessary to disentangle sex chromosome effects from gonadal hormone contributions. In this respect, the developmental timing of the dietary intervention represents an additional consideration. Although diet onset at 4 weeks of age was selected to limit obesity-related confounders while still eliciting insulin resistance [11], this window coincides with adolescence, pubertal brain maturation, and the establishment of estrogen signaling; the persistent female vulnerability we observed may therefore partly reflect an interaction between metabolic stress and hormonal/developmental maturation, rather than metabolic memory established exclusively in the adult brain. Designs restricting diet onset to adulthood, or controlling for hormonal stage, will be required to disentangle these contributions. Third, it should be noted that the perirhinal cortex, which is central to NOR [87], was not examined here; while this does not affect the molecular alterations we report, it represents a component of the recognition-memory circuitry that could help interpret our behavioral findings and that future studies may address. Fourth, in the washout paradigm, metabolic re-adaptation was characterized primarily at the molecular level and through anthropometric parameters, without direct quantification of fat and lean mass, which would provide a complementary readout in future studies. A related consideration concerns the interpretation of systemic glucose handling and its relationship with tissue-specific molecular phenotypes. Because BVRA was constitutively deleted in all tissues, the improved glucose tolerance observed in HFD-fed BVRA$^{-/-}$ F mice cannot be attributed to a specific organ or mechanism. Dedicated tissue-specific deletion or rescue models, together with functional metabolic approaches, will be required to define the relative contribution of liver, muscle, adipose tissue, and pancreas to the systemic phenotype observed here. Finally, validation in human datasets linking BVRA expression to brain insulin sensitivity and cognitive resilience across sexes would substantially strengthen the translational significance of these findings.

CRediT authorship contribution statement

Simona Lanzillotta: Writing – review & editing, Writing – original draft, Visualization, Investigation, Formal analysis, Data curation. **Valeria Sommella:** Writing – review & editing, Investigation, Formal analysis, Data curation. **Barbara Zulli:** Writing – review & editing,

Investigation, Formal analysis, Data curation. **Anna Picca:** Writing – review & editing, Methodology, Investigation, Formal analysis, Data curation. **Riccardo Calvani:** Writing – review & editing, Investigation, Formal analysis, Data curation. **Sara Pagnotta:** Writing – review & editing, Investigation, Formal analysis, Data curation. **Gabriele Paolozzi:** Writing – review & editing, Investigation, Formal analysis, Data curation. **Mathilde Charlier:** Writing – review & editing, Investigation, Formal analysis, Data curation. **Emanuele Marzetti:** Writing – review & editing, Methodology. **Flavia Agata Cimini:** Writing – review & editing. **Maria Gisella Cavallo:** Writing – review & editing. **Bindu D. Paul:** Writing – review & editing, Resources, Methodology. **D. Allan Butterfield:** Writing – review & editing. **Fabio Di Domenico:** Writing – review & editing, Resources, Investigation, Formal analysis. **Marzia Perluigi:** Writing – review & editing, Resources, Methodology, Formal analysis. **Antonella Tramutola:** Writing – review & editing, Resources, Methodology, Formal analysis. **Eugenio Barone:** Writing – review & editing, Writing – original draft, Supervision, Resources, Project administration, Methodology, Funding acquisition, Conceptualization.

Ethics declaration

This study was conducted in accordance with the following guidelines for animal welfare and/or reporting: All the experiments were performed in strict compliance with the Italian National Laws (DL 116/92), the European Communities Council Directives (86/609/EEC). Experimental protocol was approved by Italian Ministry of Health authorizations (#522/2020-PR and #426/2024-PR). All efforts were made to minimize the number of animals used in the study and their suffering. This study was approved by the Italian Ministry of Health. (Approval No. #522/2020-PR and #426/2024-PR)

Declaration of competing interest

The authors declare that they have no known competing financial interests or personal relationships that could have appeared to influence the work reported in this paper.

Acknowledgements

This work was supported by the Alzheimer's Association AARG grant #643091, by the Alzheimer''s Association RAPID grant #643091-RAPID and by the Banca d'Italia grant #1130944/22, by the Fondi Ateneo grants funded by Sapienza University # RM120172A3160B53 and # RG11916B87F55459 to E.B.

Appendix A. Supplementary data

Supplementary data to this article can be found online at https://doi.org/10.1016/j.redox.2026.104404.

Data availability

All data supporting the findings of this study are available within the article and its Supplementary Material. The source data underlying all figures are available from the corresponding author upon reasonable request.

References

[1] S.E. Arnold, et al., Brain insulin resistance in type 2 diabetes and Alzheimer disease: concepts and conundrums, Nat. Rev. Neurol. 14 (2018) 168–181, https://doi.org/10.1038/nrneurol.2017.185.
[2] W. Chen, S. Kullmann, E.M. Rhea, Expanding the understanding of insulin resistance in brain and periphery, Trends Endocrinol. Metabol. 37 (2026) 17–30, https://doi.org/10.1016/j.tem.2025.04.010.
[3] T.R. Bomfim, et al., An anti-diabetes agent protects the mouse brain from defective insulin signaling caused by Alzheimer's disease- associated Abeta oligomers, J. Clin. Investig. 122 (2012) 1339–1353, https://doi.org/10.1172/JCI57256.
[4] M.V. Lourenco, et al., TNF-alpha mediates PKR-dependent memory impairment and brain IRS-1 inhibition induced by Alzheimer's beta-amyloid oligomers in mice and monkeys, Cell Metab. 18 (2013) 831–843, https://doi.org/10.1016/j.cmet.2013.11.002.
[5] D. Kapogiannis, et al., Association of extracellular vesicle biomarkers with alzheimer disease in the Baltimore longitudinal study of aging, JAMA Neurol. 76 (2019) 1340–1351, https://doi.org/10.1001/jamaneurol.2019.2462.
[6] A. Tramutola, et al., Alteration of mTOR signaling occurs early in the progression of Alzheimer disease (AD): analysis of brain from subjects with pre-clinical AD, amnestic mild cognitive impairment and late-stage AD, J. Neurochem. 133 (2015) 739–749, https://doi.org/10.1111/jnc.13037.
[7] C. Lanzillotta, et al., Insulin resistance, oxidative stress and mitochondrial defects in Ts65dn mice brain: a harmful synergistic path in Down syndrome, Free Radic. Biol. Med. 165 (2021) 152–170, https://doi.org/10.1016/j.freeradbiomed.2021.01.042.
[8] V.A. Pandya, R. Patani, Region-specific vulnerability in neurodegeneration: lessons from normal ageing, Ageing Res. Rev. 67 (2021) 101311, https://doi.org/10.1016/j.arr.2021.101311.
[9] S. Camandola, M.P. Mattson, Brain metabolism in health, aging, and neurodegeneration, EMBO J. 36 (2017) 1474–1492, https://doi.org/10.15252/embj.201695810.
[10] J.C. Bean, et al., Sex-specific differences in mediobasal hypothalamus in response to nutritional states, Nat. Commun. 17 (2026), https://doi.org/10.1038/s41467-026-69239-w.
[11] M. Kleinert, et al., Animal models of obesity and diabetes mellitus, Nat. Rev. Endocrinol. 14 (2018) 140–162, https://doi.org/10.1038/nrendo.2017.161.
[12] A. Tramutola, F. Di Domenico, M. Perluigi, E. Barone, Biliverdin reductase-A is a key modulator in insulin signaling and metabolism, Trends Endocrinol. Metabol. (2025), https://doi.org/10.1016/j.tem.2025.08.007.
[13] P.E. Gibbs, N. Lerner-Marmarosh, A. Poulin, E. Farah, M.D. Maines, Human biliverdin reductase-based peptides activate and inhibit glucose uptake through direct interaction with the kinase domain of insulin receptor, FASEB J. 28 (2014) 2478–2491, https://doi.org/10.1096/fj.13-247015.
[14] N. Lerner-Marmarosh, et al., Human biliverdin reductase: a member of the insulin receptor substrate family with serine/threonine/tyrosine kinase activity, Proc. Natl. Acad. Sci. U. S. A. 102 (2005) 7109–7114, https://doi.org/10.1073/pnas.0502173102.
[15] C. Lanzillotta, et al., Biliverdin Reductase-A integrates insulin signaling with mitochondrial metabolism through phosphorylation of GSK3beta, Redox Biol. 73 (2024) 103221, https://doi.org/10.1016/j.redox.2024.103221.
[16] N. Lerner-Marmarosh, T. Miralem, P.E. Gibbs, M.D. Maines, Human biliverdin reductase is an ERK activator; hBVR is an ERK nuclear transporter and is required for MAPK signaling, Proc. Natl. Acad. Sci. U. S. A. 105 (2008) 6870–6875, https://doi.org/10.1073/pnas.0800750105.
[17] C. Lanzillotta, et al., BVR-A deficiency leads to autophagy impairment through the dysregulation of AMPK/mTOR axis in the brain-implications for neurodegeneration, Antioxidants 9 (2020), https://doi.org/10.3390/antiox9080671.
[18] C. Vasavda, et al., Biliverdin reductase A is a major determinant of protective NRF2 signaling, Proc. Natl. Acad. Sci. U. S. A. 122 (2025) e2513120122, https://doi.org/10.1073/pnas.2513120122.
[19] C. Vasavda, et al., Bilirubin links heme metabolism to neuroprotection by scavenging superoxide, Cell Chem. Biol. 26 (2019) 1450–1460 e1457, https://doi.org/10.1016/j.chembiol.2019.07.006.
[20] Z. Ahmad, M. Salim, M.D. Maines, Human biliverdin reductase is a leucine zipper-like DNA-binding protein and functions in transcriptional activation of heme oxygenase-1 by oxidative stress, J. Biol. Chem. 277 (2002) 9226–9232, https://doi.org/10.1074/jbc.M108239200.
[21] D.E. Stec, et al., Biliverdin reductase A (BVRA) knockout in adipocytes induces hypertrophy and reduces mitochondria in white fat of Obese mice, Biomolecules 10 (2020), https://doi.org/10.3390/biom10030387.
[22] W. Chen, et al., Absence of the biliverdin reductase-a gene is associated with increased endogenous oxidative stress, Free Radic. Biol. Med. 115 (2018) 156–165, https://doi.org/10.1016/j.freeradbiomed.2017.11.020.
[23] D.M. Gordon, et al., CRISPR Cas9-mediated deletion of biliverdin reductase A (BVRA) in mouse liver cells induces oxidative stress and lipid accumulation, Arch. Biochem. Biophys. 672 (2019) 108072, https://doi.org/10.1016/j.abb.2019.108072.
[24] V. Ceccarelli, et al., Reduced biliverdin Reductase-A expression in visceral adipose tissue is associated with adipocyte dysfunction and NAFLD in human obesity, Int. J. Mol. Sci. 21 (2020), https://doi.org/10.3390/ijms21239091.
[25] F.A. Cimini, et al., Reduced biliverdin reductase-A levels are associated with early alterations of insulin signaling in obesity, Biochim. Biophys. Acta Mol. Basis Dis. 1865 (2019) 1490–1501, https://doi.org/10.1016/j.bbadis.2019.02.021.
[26] F.A. Cimini, et al., Biliverdin reductase-A protein levels are reduced in type 2 diabetes and are associated with poor glycometabolic control, Life Sci. 284 (2021) 119913, https://doi.org/10.1016/j.lfs.2021.119913.
[27] E. Barone, et al., Oxidative and nitrosative modifications of biliverdin reductase-A in the brain of subjects with Alzheimer's disease and amnestic mild cognitive impairment, J. Alzheimers Dis. 25 (2011) 623–633, https://doi.org/10.3233/JAD-2011-110092.
[28] E. Barone, et al., Biliverdin reductase–a protein levels and activity in the brains of subjects with Alzheimer disease and mild cognitive impairment, Biochim. Biophys. Acta 1812 (2011) 480–487, https://doi.org/10.1016/j.bbadis.2011.01.005.

[29] F.A. Cimini, et al., Dynamic changes of BVRA protein levels occur in response to insulin: a pilot study in humans, Int. J. Mol. Sci. 24 (2023), https://doi.org/10.3390/ijms24087282.
[30] J. Kapitulnik, M.D. Maines, Pleiotropic functions of biliverdin reductase: cellular signaling and generation of cytoprotective and cytotoxic bilirubin, Trends Pharmacol. Sci. 30 (2009) 129–137, https://doi.org/10.1016/j.tips.2008.12.003.
[31] B. Wegiel, et al., Biliverdin inhibits toll-like receptor-4 (TLR4) expression through nitric oxide-dependent nuclear translocation of biliverdin reductase, Proc. Natl. Acad. Sci. U. S. A. 108 (2011) 18849–18854, https://doi.org/10.1073/pnas.1108571108.
[32] P.E. Gibbs, T. Miralem, M.D. Maines, Characterization of the human biliverdin reductase gene structure and regulatory elements: promoter activity is enhanced by hypoxia and suppressed by TNF-alpha-activated NF-kappaB, FASEB J. 24 (2010) 3239–3254, https://doi.org/10.1096/fj.09-144592.
[33] S. Gargiulo, et al., Evaluation of growth patterns and body composition in C57Bl/6J mice using dual energy X-ray absorptiometry, Biomed Res. Int. (2014) 253067, https://doi.org/10.1155/2014/253067, 2014.
[34] M. Spinelli, et al., Brain insulin resistance impairs hippocampal synaptic plasticity and memory by increasing GluA1 palmitoylation through FoxO3a, Nat. Commun. 8 (2009), https://doi.org/10.1038/s41467-017-02221-9, 2017.
[35] F. Natale, et al., Inhibition of zDHHC7-driven protein S-palmitoylation prevents cognitive deficits in an experimental model of Alzheimer's disease, Proc. Natl. Acad. Sci. U. S. A. 121 (2024) e2402604121, https://doi.org/10.1073/pnas.2402604121.
[36] D. Valenti, L. de Bari, B. De Filippis, L. Ricceri, R.A. Vacca, Preservation of mitochondrial functional integrity in mitochondria isolated from small cryopreserved mouse brain areas, Anal. Biochem. 444 (2014) 25–31, https://doi.org/10.1016/j.ab.2013.08.030.
[37] M.S. Winzell, B. Ahren, The high-fat diet-fed mouse: a model for studying mechanisms and treatment of impaired glucose tolerance and type 2 diabetes, Diabetes 53 (Suppl 3) (2004) S215–S219, https://doi.org/10.2337/diabetes.53.suppl_3.s215.
[38] T.D. Hinds Jr., et al., Biliverdin reductase A attenuates hepatic steatosis by inhibition of Glycogen Synthase Kinase (GSK) 3beta phosphorylation of serine 73 of peroxisome proliferator-activated receptor (PPAR) alpha, J. Biol. Chem. 291 (2016) 25179–25191, https://doi.org/10.1074/jbc.M116.731703.
[39] M. Hallschmid, Intranasal insulin, J. Neuroendocrinol. 33 (2021) e12934, https://doi.org/10.1111/jne.12934.
[40] S. Craft, et al., Intranasal insulin therapy for Alzheimer disease and amnestic mild cognitive impairment: a pilot clinical trial, Arch. Neurol. 69 (2012) 29–38, https://doi.org/10.1001/archneurol.2011.233.
[41] K. Yang, et al., The key roles of GSK-3beta in regulating mitochondrial activity, Cell. Physiol. Biochem. 44 (2017) 1445–1459, https://doi.org/10.1159/000485580.
[42] E. Barone, E. Head, D.A. Butterfield, M. Perluigi, HNE-modified proteins in Down syndrome: involvement in development of Alzheimer disease neuropathology, Free Radic. Biol. Med. 111 (2017) 262–269, https://doi.org/10.1016/j.freeradbiomed.2016.10.508.
[43] A. Tramutola, et al., Polyubiquitinylation profile in Down syndrome brain before and after the development of alzheimer neuropathology, Antioxid. Redox Signaling 26 (2017) 280–298, https://doi.org/10.1089/ars.2016.6686.
[44] E. Barone, et al., Biliverdin Reductase-A mediates the beneficial effects of intranasal insulin in alzheimer disease, Mol. Neurobiol. 56 (2019) 2922–2943, https://doi.org/10.1007/s12035-018-1231-5.
[45] C. Mancuso, R. Siciliano, E. Barone, Curcumin and Alzheimer disease: this marriage is not to be performed, J. Biol. Chem. 286 (2011) le3, https://doi.org/10.1074/jbc.L110.133520 author reply le4.
[46] A.J.T. Yang, et al., Differences in inflammatory markers, mitochondrial function, and synaptic proteins in male and female Alzheimer's disease post mortem brains, Alzheimer's Dement. 21 (2025) e70645, https://doi.org/10.1002/alz.70645.
[47] W. Chen, X. Liu, V.R. Munoz, C.R. Kahn, Loss of insulin signaling in microglia impairs cellular uptake of Abeta and neuroinflammatory response exacerbating AD-like neuropathology, Proc. Natl. Acad. Sci. U. S. A. 122 (2025) e2501527122, https://doi.org/10.1073/pnas.2501527122.
[48] K. Wardelmann, et al., Insulin action in the brain regulates mitochondrial stress responses and reduces diet-induced weight gain, Mol. Metabol. 21 (2019) 68–81, https://doi.org/10.1016/j.molmet.2019.01.001.
[49] S. Kullmann, et al., Central nervous pathways of insulin action in the control of metabolism and food intake, Lancet Diabetes Endocrinol. 8 (2020) 524–534, https://doi.org/10.1016/S2213-8587(20)30113-3.
[50] D. Garcia, R.J. Shaw, AMPK: mechanisms of cellular energy sensing and restoration of metabolic balance, Mol. Cell 66 (2017) 789–800, https://doi.org/10.1016/j.molcel.2017.05.032.
[51] E. Trefts, R.J. Shaw, AMPK: restoring metabolic homeostasis over space and time, Mol. Cell 81 (2021) 3677–3690, https://doi.org/10.1016/j.molcel.2021.08.015.
[52] S. Wang, J. Tan, Y. Miao, Q. Zhang, Mitochondrial dynamics, mitophagy, and mitochondria-endoplasmic reticulum contact sites crosstalk under hypoxia, Front. Cell Dev. Biol. 10 (2022) 848214, https://doi.org/10.3389/fcell.2022.848214.
[53] S. Herzig, R.J. Shaw, AMPK: guardian of metabolism and mitochondrial homeostasis, Nat. Rev. Mol. Cell Biol. 19 (2018) 121–135, https://doi.org/10.1038/nrm.2017.95.
[54] L. Goedeke, et al., High-fat-diet-induced hepatic insulin resistance per se attenuates murine de novo lipogenesis, iScience 27 (2024) 111175, https://doi.org/10.1016/j.isci.2024.111175.
[55] T. Bo, et al., Hepatic selective insulin resistance at the intersection of insulin signaling and metabolic dysfunction-associated steatotic liver disease, Cell Metab. 36 (2024) 947–968, https://doi.org/10.1016/j.cmet.2024.04.006.
[56] J. Zhang, Z. Gao, J. Yin, M.J. Quon, J. Ye, S6K directly phosphorylates IRS-1 on Ser-270 to promote insulin resistance in response to TNF-(Alpha) signaling through IKK2, J. Biol. Chem. 283 (2008) 35375–35382, https://doi.org/10.1074/jbc.M806480200.
[57] L.R. Pearce, D. Komander, D.R. Alessi, The nuts and bolts of AGC protein kinases, Nat. Rev. Mol. Cell Biol. 11 (2010) 9–22, https://doi.org/10.1038/nrm2822.
[58] A. Levina, K.D. Fleming, J.E. Burke, T.A. Leonard, Activation of the essential kinase PDK1 by phosphoinositide-driven trans-autophosphorylation, Nat. Commun. 13 (2022) 1874, https://doi.org/10.1038/s41467-022-29368-4.
[59] L. Wagner, et al., Brain insulin responsiveness is linked to age and peripheral insulin sensitivity, Diabetes Obes. Metabol. 25 (2023) 2171–2180, https://doi.org/10.1111/dom.15094.
[60] C. Koliaki, et al., Adaptation of hepatic mitochondrial function in humans with non-alcoholic fatty liver is lost in steatohepatitis, Cell Metab. 21 (2015) 739–746, https://doi.org/10.1016/j.cmet.2015.04.004.
[61] S. Satapati, et al., Elevated TCA cycle function in the pathology of diet-induced hepatic insulin resistance and fatty liver, J. Lipid Res. 53 (2012) 1080–1092, https://doi.org/10.1194/jlr.M023382.
[62] B. Dewidar, et al., Alterations of hepatic energy metabolism in murine models of obesity, diabetes and fatty liver diseases, EBioMedicine 94 (2023) 104714, https://doi.org/10.1016/j.ebiom.2023.104714.
[63] Y. Li, R. Ma, X. Hao, Therapeutic role of PTEN in tissue regeneration for management of neurological disorders: stem cell behaviors to an in-depth review, Cell Death Dis. 15 (2024) 268, https://doi.org/10.1038/s41419-024-06657-y.
[64] N. Turner, L.K. Heilbronn, Is mitochondrial dysfunction a cause of insulin resistance? Trends Endocrinol. Metabol. 19 (2008) 324–330, https://doi.org/10.1016/j.tem.2008.08.001.
[65] S. Lanzillotta, L.R. Rolfi, B. Zulli, E. Barone, Metabolic breakdown: linking insulin resistance and mitochondrial dysfunction to neurodegeneration in Alzheimer's disease, Neural Regen. Res. 21 (2026) 2227–2237, https://doi.org/10.4103/NRR.NRR-D-25-00144.
[66] M. Schell, K. Wardelmann, A. Kleinridders, Untangling the effect of insulin action on brain mitochondria and metabolism, J. Neuroendocrinol. 33 (2021) e12932, https://doi.org/10.1111/jne.12932.
[67] A. Fernandez, et al., Sex differences in the progression to Alzheimer's disease: a combination of functional and structural markers, GeroScience 46 (2024) 2619–2640, https://doi.org/10.1007/s11357-023-01020-z.
[68] M.A. O'Neal, Women and the risk of Alzheimer's disease, Front. Glob. Women Health 4 (2023) 1324522, https://doi.org/10.3389/fgwh.2023.1324522.
[69] J.M. Eissman, et al., Sex differences in the genetic architecture of cognitive resilience to Alzheimer's disease, Brain 145 (2022) 2541–2554, https://doi.org/10.1093/brain/awac177.
[70] C. Lopez-Lee, E.R.S. Torres, G. Carling, L. Gan, Mechanisms of sex differences in Alzheimer's disease, Neuron 112 (2024) 1208–1221, https://doi.org/10.1016/j.neuron.2024.01.024.
[71] C. Vasavda, et al., Biliverdin reductase bridges focal adhesion kinase to Src to modulate synaptic signaling, Sci. Signal. 15 (2022) eabh3066, https://doi.org/10.1126/scisignal.abh3066.
[72] B.D. Winters, L.M. Saksida, T.J. Bussey, Object recognition memory: neurobiological mechanisms of encoding, consolidation and retrieval, Neurosci. Biobehav. Rev. 32 (2008) 1055–1070, https://doi.org/10.1016/j.neubiorev.2008.04.004.
[73] A. Ghazizadeh, S. Hong, O. Hikosaka, Prefrontal cortex represents long-term memory of object values for months, Curr. Biol. 28 (2018) 2206–2217 e2205, https://doi.org/10.1016/j.cub.2018.05.017.
[74] E. Barone, D.A. Butterfield, Insulin signaling in microglia: a metabolic switch controlling neuroinflammation and amyloid pathology in Alzheimer's disease, Cell Metab. 37 (2025) 1630–1632, https://doi.org/10.1016/j.cmet.2025.06.005.
[75] J. Chen, et al., AMPK/SIRT1/PGC-1alpha signaling pathway: molecular mechanisms and targeted strategies from energy homeostasis regulation to disease therapy, CNS Neurosci. Ther. 31 (2025) e70657, https://doi.org/10.1111/cns.70657.
[76] P. Gaignard, et al., Effect of sex differences on brain mitochondrial function and its suppression by ovariectomy and in aged mice, Endocrinology 156 (2015) 2893–2904, https://doi.org/10.1210/en.2014-1913.
[77] C. Arias-Reyes, K. Losantos-Ramos, M. Gonzales, D. Furrer, J. Soliz, NADH-linked mitochondrial respiration in the developing mouse brain is sex-, age- and tissue-dependent, Respir. Physiol. Neurobiol. 266 (2019) 156–162, https://doi.org/10.1016/j.resp.2019.05.011.
[78] S. Kullmann, et al., A short-term, high-caloric diet has prolonged effects on brain insulin action in men, Nat. Metab. 7 (2025) 469–477, https://doi.org/10.1038/s42255-025-01226-9.
[79] Y. Lv, et al., Healthy dietary patterns, longevity genes, and life expectancy: a prospective cohort study, Sci. Adv. 12 (2026) eads7559, https://doi.org/10.1126/sciadv.ads7559.
[80] X. Ma, et al., Molecular mechanisms in liver repair and regeneration: from physiology to therapeutics, Signal Transduct. Targeted Ther. 10 (2025) 63, https://doi.org/10.1038/s41392-024-02104-8.
[81] W.H. Lee, S.M. Najjar, C.R. Kahn, T.D. Hinds Jr., Hepatic insulin receptor: new views on the mechanisms of liver disease, Metabolism 145 (2023) 155607, https://doi.org/10.1016/j.metabol.2023.155607.

[82] W.H. Lee, et al., The physiology of MASLD: molecular pathways between liver and adipose tissues, Clin. Sci. (Lond.) 139 (2025) 1015–1046, https://doi.org/10.1042/CS20257571.
[83] R.S. Rector, et al., Mitochondrial dysfunction precedes insulin resistance and hepatic steatosis and contributes to the natural history of non-alcoholic fatty liver disease in an obese rodent model, J. Hepatol. 52 (2010) 727–736, https://doi.org/10.1016/j.jhep.2009.11.030.
[84] A. Franko, et al., Liver adapts mitochondrial function to insulin resistant and diabetic states in mice, J. Hepatol. 60 (2014) 816–823, https://doi.org/10.1016/j.jhep.2013.11.020.
[85] J. Zhu, Y. Zhou, B. Jin, J. Shu, Role of estrogen in the regulation of central and peripheral energy homeostasis: from a menopausal perspective, Ther. Adv. Endocrinol. Metab. 14 (2023) 20420188231199359, https://doi.org/10.1177/20420188231199359.
[86] A.S. Shulha, et al., An update on the role of sex hormones in the function of the cardiorenal mitochondria, Biochem. Soc. Trans. 52 (2024) 2307–2319, https://doi.org/10.1042/BST20240046.
[87] M.W. Brown, J.P. Aggleton, Recognition memory: what are the roles of the perirhinal cortex and hippocampus? Nat. Rev. Neurosci. 2 (2001) 51–61, https://doi.org/10.1038/35049064.